EXPANDING AND ENHANCING THE CAPABILITIES OF THE QUADRUPOLE ION TRAP MASS SPECTROMETER FOR HIGH RESOLUTION AND MS^n ANALYSES

By

JOSEPH JAMES MULHOLLAND

A DISSERTATION PRESENTED TO THE GRADUATE SCHOOL
OF THE UNIVERSITY OF FLORIDA IN PARTIAL FULFILLMENT
OF THE REQUIREMENTS FOR THE DEGREE OF
DOCTOR OF PHILOSOPHY

UNIVERSITY OF FLORIDA

2000

This is dedicated to all of the members of the Mulholland family who have struggled to provide more opportunities for their children than life offered them.

ACKNOWLEDGEMENTS

I'd like to thank all of the little people who have helped to make this possible. There are many who are deserving of my thanks and I hope that they all share in this achievement.

First, I would like to thank Mohammed Iqbal for encouraging me to return to school. It may have taken awhile, but his constant prodding did not fall on deaf ears.

Secondly, I'd like to express my gratitude to my advisor, Rick Yost, especially for finding a funded project to put me on when I couldn't bear one more semester of teaching. Without AWWARF, I don't think I would have made it.

I'd also like to thank the members of the Yost group. Specifically, Rick Troendle, who joined the Yost group at the same time I did, for always trailblazing a path through the graduate school maze which I could follow. He and Kevin McHale have helped to contribute to my understanding of the fundamentals of the ion trap, as well as many other topics, through insightful "discussions". It is true that some may call them arguments— and no one denies that there were many hotly debated issues (maintaining carbonation in soda, for example)— but we were only reflecting the passion of our arguments in the volume of our voices.

Additionally, I like to thank Joe McClellan, who shared the LCQ with me. It was a true division of labor that worked well for four years. I could always count on a full tank of nitrogen being nearby (unlabeled and indistinguishable from the empty tanks, but it was nearby!).

Of course, I cannot mention Joe without mentioning his fellow Holy Cross graduate, Jim Murphy (Yes, Jim, your acknowledgement streak is intact!). Jim is always there with a kind word of encouragement and a fresh perspective. After the numerous celebrations at the Lone Star Steakhouse with our friends, I'm sure I'll never be able to look at a plate of cheese fries without thinking about Murf.

Similarly, I will be reminded of Murf's sidekick, and our honorary lab member, T.J. Banisaukas, everytime I hear a terrible joke. T.J. is the ultimate webble-wobble when it comes to humor; he doesn't care if you don't laugh at his jokes, he just keeps putting them out there. You have to admire his tenacity.

I'd also like to thank Josh, Beth, Mike, Todd, Andy, Rich, Giselle and all the rest of the Yost group for making it an interesting four years. I'd especially like to thank T.P. and C.L. (you know who you are!) for an incredibly entertaining ASMS 2000, which will not be forgotten.

Finally, I wish to express my sincerest gratitude to my family. Their moral (and sometimes financial) support allowed me to pursue, and attain, my dream of becoming a doctor. I hope that I'm just the start.

TABLE OF CONTENTS

page

ACKNOWLEDGMENTS iii

LIST OF FIGURES vii

ABSTRACT x

AN INTRODUCTION TO ION TRAPS 1

- Overview of the Quadrupole Ion Trap 1
- The Finnigan MAT LCQ 7
  - Ionization 7
  - Ion Optics 10
  - The LCQ Ion Trap 10
  - Ion Ejection 11
  - Ion Detection 12

THE DEVELOPMENT OF MULTI-LEVEL CID AS AN ENHANCEMENT FOR MS^n ANALYSES 19

- Introduction to MS/MS and MS^n 19
- The Basics of Tandem MS on an Ion Trap 20
  - The Excitation q 20
  - Psuedo-potential Well Depth 21
  - Excitation 21
  - Mass Analysis 22
- Problems with LC/MS^n Analyses 22
- The Development of Multi-level CID 24
  - Preliminary Work 25
  - Determining Additional CID Voltages 25
  - Modeling Multi-level CID Behavior Mathematically 27
  - Automating Multi-level CID 28
  - Parameters for Automated Multi-level CID 30
  - A False Premise 32
  - Problems with Well depth 34
  - A New Solution 35
- Final Testing of Multi-level CID 37
  - Normalized Collision Energy 37

Comparison of CID Techniques 38
Conclusions for Multi-level CID 39

HIGH RESOLUTION 63

Overview of High Resolution on the Ion Trap 63
Difficulties with High Resolution 66
Early High Resolution Work with the LCQ 67
Resolving Power vs. Resolution 70
Frequency Sweeps 72
Final Results of High Resolution on the LCQ 73
Vernier DAC 73
Development of A Novel Ion Ejection Technique 74
Comparison of HI-RES to Mass-selective Instability 77

CONCLUSIONS AND FUTURE WORK 104

LIST OF REFERENCES 107

BIOGRAPHICAL SKETCH 109

LIST OF FIGURES

Figure Page

Figure 1-1. The quadrupole ion trap. 13

Figure 1-2. Changes in the trapping field due to the phase of the main r.f.............................14

Figure 1-3. A representation of the psuedo-potential well. 15

Figure 1-4. The Mathieu stability diagram. 16

Figure 1-5. A diagram of the Finnigan MAT LCQ. 17

Figure 1-6. A mass spectrum of angiotensin I showing the +2 charge state (the $[M+2H]^{+2}$ ion). 18

Figure 2-1. A cartoon of a Fourier transformation of the isolation waveform of the LCQ. .41

Figure 2-2. A collision energy curve for the $[M+H]^+$ ion of caffeine.....................................42

Figure 2-3. Collision energy curves for $[M+H]^+$ and $[M+Na]^+$ ions of erythromycin. 43

Figure 2-4. Scan function plots for multi-level and single-level CID. 44

Figure 2-5. Collision energy curve for the $[M+H]^+$ ion of benzamide using single-level and multi-level CID. 45

Figure 2-6. Single-level and multi-level CID of the $[M+Na]^+$ of gramicidin A...................46

Figure 2-7. Collision energy curves for the $[M+H]^+$ ion of gramicidin A with a fourth level of CID..47

Figure 2-8. The effects of changing the second multi-level CID coefficient. 48

Figure 2-9. A comparison of predicted and actual collision energy curves for caffeine using four-level CID. 49

Figure 2-10. A comparison of predicted and actual collision energy curves for caffeine using ten levels of CID. 50

Figure 2-11. Intensity of product ion as a function of the number of CID levels.................51

Figure 2-12. An LC/MS/MS analysis of PEG 600 obtained using multi-level CID. 52

Figure 2-13. CID efficiency for multi-level CID and single-level CID. 53

Figure 2-14. A simulation of the depth of the the psuedo-potential well 54

Figure 2-15. Survivor ion curves for the $[M+H]^+$ of benzimidizole...................................55

Figure 2-16. The well-depth curve for the $[M+H]^+$ ion of benzimidazole by resonance ejection...56

Figure 2-17. The well-depth curve for the $[M+H]^+$ ion of benzimidazole by resonance excitation...57

Figure 2-18. The well-depth curve for iodide (m/z 127). 58

Figure 2-19. A plot of the voltage necessary to eject 50% of the $[M+Na]^+$ ions of PEGs...59

Figure 2-20. A linear fit of voltage to the sodiated PEGs data. 60

Figure 2-21. A comparison of CID techniques on a tryptic peptide of myoglobin (m/z 749.4) 61

Figure 2-22. A comparison of CID techniques on a tryptic peptide of myoglobin (m/z 1378.7) 62

Figure 3-1. Peak width as a function of scan rate for caffeine. 81

Figure 3-2. Peak width as a function of resonance ejection amplitude. 82

Figure 3-3. Peak width as a function of scan rate for 4-(*p*-nitrobenzyl)-pyridine. 83

Figure 3-4. Peak width versus ion injection time for caffeine...84

Figure 3-5. Linearity curves for caffeine. 85

Figure 3-6. Mass spectrum (uncalibrated) of caffeine and glucuronic acid. 86

Figure 3-7. Mass spectrum (uncalibrated) of caffeine and glucuronic acid with additional caffeine..87

Figure 3-8. Overlay of DAC step size with mass spectrum of caffeine and glucuronic acid...88

Figure 3-9. Mass spectrum of caffeine obtained using a resonance ejection frequency sweep..89

Figure 3-10. Mass spectra of caffeine acquired without (a) and with (b) the vernier DAC. 90

Figure 3-11. Peak width as a function of scan rate for caffeine. 91

Figure 3-12. An illustration of HI-RES. 92

Figure 3-13. Frequency versus time plot for HI-RES. 93

Figure 3-14. Frequency versus time plot for mass-selective instability with resonance ejection. 94

Figure 3-15. Zoomscan and HI-RES spectra of the $[M+5H]^{+5}$ ion of bovine insulin. 95

Figure 3-16. HI-RES spectrum of cytochrome c $[M+8H]^{+8}$. 96

Figure 3-17. HI-RES spectrum of myoglobin $[M+12H]^{+12}$. 97

Figure 3-18. HI-RES of cytochrome c $[M+15H]^{+15}$. 98

Figure 3-19. HI-RES spectrum of cytochrome c $[M+18]^{+18}$ 99

Figure 3-20. HI-RES spectrum of myoglobin $[M+20H]^{+20}$. 100

Figure 3-21. The effect of space charge on peak widths. 101

Figure 3-22. Peak widths as a function of scan rate. 102

Figure 3-23. Peak width as a function of ion trap bath gas pressure. 103

Abstract of Dissertation Presented to the Graduate School
of the University of Florida in Partial Fulfillment of the
Requirements for the Degree of Doctor of Philosophy

EXPANDING AND ENHANCING THE CAPABILITIES OF THE QUADRUPOLE ION TRAP MASS SPECTROMETER FOR HIGH RESOLUTION AND MS^n ANALYSES

By
JOSEPH JAMES MULHOLLAND

August 2000

Chairman: Richard A. Yost
Major Department: Chemistry

The quadrupole ion trap mass spectrometer has been shown to be a versatile tool for the analytical chemist since its commercialization over fifteen years ago. Despite its demonstrated abilities, areas for improvement still remain. This work focused on two such areas: routinely obtaining the high resolutions necessary to implement exact mass measurement on the ion trap; and developing a method of producing reproducible and informative product ion spectra from collision-induced dissociation.

After careful study of how ions can be ejected from an ion trap with high resolution using conventional ejection techniques, a novel way of ejecting ions with enhanced resolution was developed and refined. In contrast to the conventional ion ejection techniques, this new technique was shown to be very tolerant of the pressure of the buffer gas present in the ion trap. It was also shown to be capable of resolving isotopic envelopes that were incapable of being resolved using conventional methods.

With this development, the ion trap is now capable of attaining the resolutions necessary for exact mass measurement.

Additionally, the process of generating fragment ions from a selected precursor ion was studied and ultimately improved upon. Formerly, a single excitation voltage was applied to the ion of interest in order to generate energetic collisions with the buffer gas present in the ion trap. This was an inefficient means of generating informative fragment ions since selecting the correct excitation voltage depends on many parameters. An improved approach was developed where a series of increasing excitation voltages are applied to the ion of interest such that the probability of generating fragment ions is greatly enhanced without *a priori* knowledge of an appropriate excitation voltage.

Together, these two advancements help to expand and enhance the capabilities of the quadrupole ion trap mass spectrometer so that it may continue to be a powerful tool for analytical chemists in the future.

CHAPTER 1
AN INTRODUCTION TO ION TRAPS

The quadrupole ion trap has evolved from a simple storage device for charged particles used by select physicists into one of the most versatile mass spectrometers available today. Since its commercialization in 1984 by Finnigan MAT (Stafford et al., 1984), numerous technical advances have helped to push the quadrupole ion trap into the forefront of benchtop mass spectrometry. This dissertation will focus on two areas of development: specifically, high resolution and improved MS^n capability. Of course, technical advances can arise only from a thorough understanding of the fundamental principles at the heart of an invention. Therefore, this chapter is intended as a primer for understanding the basic operating parameters of the quadrupole ion trap: it is by no means an exhaustive review, as such reviews already have been published by others (March & Hughes, 1989 and March & Todd, 1995).

Overview of the Quadrupole Ion Trap

The quadrupole ion trap is so named because of the quadrupolar field that is established within the confines of the trap. Though there are numerous ways to establish a quadrupolar field through various electrode geometries, only one method has been popularized. The commercial ion trap is made up of three hyperbolic electrodes: one ring electrode and two endcap electrodes (Figure 1-1). The quadrupolar field is generated by establishing a potential difference between the ring electrode and the endcap electrodes. An AC voltage with amplitude (zero-to-peak), V, and angular frequency, Ω, is placed on the ring electrode with an optional DC voltage, *U* (March and Hughes, 1989). Thus, a dynamically changing trapping field is established due to the oscillating nature of the AC voltage (also known as r.f. since the frequency of the AC voltage lies in the radio frequency range).

Figure 1-2 shows how the potential of the trapping field varies with the phase of the r.f. voltage being placed on the ring electrode. The potential of the quadrupolar trapping field is similar to the shape of a saddle; it varies quadratically with displacement from the center of the trap. When the ring experiences a positive voltage, a positive ion is repelled and wants to travel in the direction of lowest potential (down hill) which is toward either endcap. The phase of the main r.f. quickly changes though. Approximately one microsecond later, the ring electrode is negative and attractive to a positive ion, causing a reversal in the direction of the ion.

Although the potential of the field varies quadratically, the electric field strength varies linearly with the displacement from the center of the field (March and Hughes, 1989). Since the center of the field corresponds to the center of the ion trap, this means that ions will experience increasing field strength as they move from the center of the trap. Conversely, if an ion can be brought to the center of the ion trap, it will not experience the field at all (March and Hughes, 1989). This forms the basis of an ion trap's ability to hold ions. Unfortunately, it also reveals the difficulty of trapping ions that were formed external to the ion trap itself.

If an ion has enough kinetic energy to penetrate the trapping field on the way into the ion trap, then it will also have enough kinetic energy to break through the field and exit the ion trap on the other side. Classically, the ion trap is represented as a potential well in which an ion can be contained (Figure 1-3a) (Major and Dehmelt, 1968). When an ion enters the well, it picks up enough kinetic energy to make it out the other side (Figure 1-3b). Fortunately, there are ways to remove some of the ion's kinetic energy so that it will not be able to escape the well.

The most common way of removing excess kinetic energy from an ion is by flooding the ion trap with a light buffer gas such as helium. The helium, which is not ionized, is not subject to the electric field of the ion trap and as such can fill the volume of the trap. When ions come into the trap, they are subjected to collisions with the helium. These collisions are a source of friction and cause the ions to slow down such that they can be captured by the oscillating r.f. trapping field (McLuckey et al., 1989).

Once captured by the trapping field, ions begin to adopt periodic motions in the ion trap based on parameters such as the size of the trap, the mass of the ion, etc. Amazingly, these motions can be described by the solutions of a second-order linear differential equation derived by the mathematician Mathieu in 1868 (Mathieu, 1868).

The standard form of the Mathieu equation is

$$\frac{\partial^2 \mathrm{u}}{\partial \xi^2} + (\mathrm{a_u} - 2\mathrm{q_u} \cos 2\xi)\mathrm{u} = 0 \tag{1-1}$$

where $\xi = \Omega t/2$ and u is the position of the ion in either the radial (u=r) or the axial (u=z) direction (March and Hughes, 1989). The reduced parameters a_u and q_u are given by the equations (March and Hughes, 1989) below:

$$a_z = -2a_r = \frac{-16eU}{m\Omega^2 (r_0^2 + 2z_0^2)} \tag{1-2}$$

$$q_z = -2q_r = \frac{-8eV}{m\Omega^2 (r_0^2 + 2z_0^2)} \tag{1-3}$$

where:

e is the charge of an electron (1.602 x 10^{-19} C)

m is the mass of the ion (in kg, kg mol^{-1}/6.022 x 10^{23} mol^{-1})

U and V are $volts_{(0-p)}$ (1 V= kg m^2 s^{-2} C^{-1})

Ω=2πf (f is the drive frequency in s^{-1})

r_0 and z_0 are the dimensions of the trap (m).

(Note: Equation 1-2 and 1-3 assume that there is only a single charge on the ion of mass, m. Frequently, ionization techniques can deposit more than one charge on an ion. Mass spectrometers actually measure a mass-to-charge ratio, m/z, where z is the number of charges on the ion: it should not be confused with z_0, the axial dimension of the ion trap.)

Of course, not all ions can be trapped for a given set of experimental conditions. In order to be trapped, an ion must adopt a stable trajectory within the volume of the ion trap. This requires that the ion be stable in both the axial and radial directions and that it not strike one of the electrodes during its maximum excursions from the trap center. The parameters a_u and q_u determine whether or not an ion will be stable. A graphical representation of these parameters, commonly referred to as the Mathieu stability diagram, appears in Figure 1-4. It is interesting to note that numerous stability regions exist based on values of a_u and q_u (March and Hughes, 1989), but all of the work in this dissertation was done in the stability region shown in Figure 1-4.

Another important fundamental parameter of an ion's motion is β. β is related to the fundamental secular frequency (ω) of an ion's motion (March and Hughes, 1989) by

$$\omega_u = \beta_u \frac{\Omega}{2}. \qquad (1\text{-}4)$$

The fundamental secular frequency of an ion's motion is the frequency at which it travels from one maximum excursion from the center of the trap to the other and back again in either the axial or radial direction. For example, if dealing with the axial direction, the fundamental secular frequency (ω_z) would be the frequency with which the ion travels from the entrance endcap to the exit endcap and back to the entrance endcap again. The fundamental secular frequency of an ion's motion is extremely important to mass spectrometrists since it is the primary way to manipulate the motion of particular ions when conducting experiments in an ion trap.

It is apparent from equation 1-4 that β needs to be calculated before the fundamental secular frequency can be determined. β is related to both a_u and q_u, but can not be calculated directly. Dehmelt worked out an approximation of β that works well at $q<0.4$, but is invalid at higher q. The method of successive approximations is the most accurate way to determine β (March and Hughes, 1989) and is given below:

$$\beta^2 = a + \cfrac{q^2}{(2+\beta)^2 - a - \cfrac{q^2}{(4+\beta)^2 - a - \cfrac{q^2}{(6+\beta)^2 - a - ...etc.}}}$$

$$+ \cfrac{q^2}{(\beta-2)^2 - a - \cfrac{q^2}{(\beta-4)^2 - a - \cfrac{q^2}{(\beta-6)^2 - a - ...etc.}}} \qquad (1\text{-}5)$$

Finally, another equation that often is not written explicitly makes it much easier to deal with ion trap experiments. On a given instrument, the size of the trap is fixed, so

r_0 and z_0 are constant. Additionally, the drive frequency, Ω, is fixed on all commercial ion trap instruments. Applying these facts to Equation 1-3, the following is obtained:

$$q_z = \frac{-8e}{\Omega^2(r_0^2 + 2z_0^2)} * \frac{V}{m} = k * \frac{V}{m} \tag{1-6}$$

where k is a simple constant dependent on the instrument. Rearrangement of 1-6 yields:

$$mq_z = k * V \tag{1-7}$$

Now, for a given voltage, V, the product of m and q is also a constant. Therefore, at a given voltage, V, q_z can be calculated for any mass, m (or more correctly, mass-to-charge ratio). This can be further extrapolated such that for any mass, m_1, at a known q value, q_1, the mass, m_2, or the q value, q_2, can be calculated from the following:

$$m_1 q_1 = m_2 q_2 \tag{1-8}$$

Equation 1-8 is a very useful equation for calculating a mass at a particular q of interest (or q for a particular mass of interest) when any other mass and its q value are known. For example, it is often necessary to calculate the low-mass cut-off (LMCO) of the ion trap for a particular set of conditions. The LMCO is the smallest mass-to-charge that will be held stable in the ion trap. When operating along the a_z=0 line of the Mathieu stability diagram, the LMCO will be at a q_z=0.908 since this is the highest q that maintains both axial and radial stability. For example, if mass-to-charge (m/z) 500 is placed at a q_z=0.1, equation 1-8 can be used to calculate the mass-to-charge that would occupy a q_z=0.908 to determine the LMCO.

$$500 * 0.1 = m_2 * 0.908$$

$$m_2 = \frac{500 * 0.1}{0.908} = 55$$

The LMCO is m/z 55 when m/z 500 is placed at a q_z=0.1.

The Finnigan MAT LCQ

Except where noted, all work in this dissertation was conducted on the Finnigan MAT LCQ LC/MS^n instrument. As such, it is important to have an understanding of this instrument and how it is configured. A schematic of the instrument is shown in Figure 1-5 and will be discussed in further detail below.

Ionization

All mass spectrometers measure the mass-to-charge ratio of ions: neutral molecules must be charged (ionized) before measurements can be made. The LCQ is equipped with two atmospheric pressure ionization sources. One is an electrospray ionization (ESI) source; the other is an atmospheric pressure chemical ionization (APCI) source. Unless otherwise noted, all of the work reported here was conducted using the ESI source.

Electrospray is a unique ionization technique. It is the only technique where multiple charges may be readily deposited onto a single molecule (Cole, 1997). As previously mentioned, mass spectrometers measure mass-to-charge ratio (m/z), not mass. All other ionization techniques typically deposit only one charge per molecule, so measuring the mass-to-charge ratio is therefore equivalent to measuring the molecule's mass. With electrospray, the charge, z, is no longer limited to one because of the way in which electrospray forms ions.

During electrospray ionization, a high voltage is applied to a condensed-phase (liquid) sample. In the LCQ, the voltage (~4 kV) is applied to a stainless steel needle (26 ga, 460 μm o.d., 260 μm i.d.) that surrounds a piece of 100 μm i.d., 197 μm o.d. fused silica where the sample to be analyzed is flowing. The high voltage causes the formation of charged droplets at the tip of the needle. A coaxial flow of nitrogen sheath gas is passed through the needle (around the fused silica) to aid in the formation of droplets.

It is important to note that the droplets are being formed at atmospheric pressure. Unfortunately, mass spectrometers need to operate under vacuum (Watson, 1985). This means that an interface between the high pressure of the atmosphere and the low pressure of the vacuum must be used to conduct the droplets into the mass spectrometer.

The droplets, which contain solvent and analyte molecules, are directed toward a heated stainless steel capillary which is the inlet to the vacuum system. The capillary is heated in order to help desolvate electrosprayed droplets. Desolvating removes the solvent molecules, leaving the analyte molecules and charges behind. With the solvent removed, the analyte molecules retain the charge(s) and can be transported further into the vacuum chamber as ions. Transporting the ions further into the vacuum chamber will be discussed below in the ion optics section.

Here, it is worth stating that multiple charges on a molecule can be advantageous, but also troublesome.

The advantage of having multiple charges on a single molecule is that the mass spectrometer can now measure masses for molecules that were once beyond its capability. The LCQ has the ability to scan up to m/z 2000. Using other ionization techniques, the LCQ is effectively limited to measuring masses less than 2000 Daltons (Da; a unit of mass equal to 1/12 of ^{12}C atom) (Watson, 1985) without resorting to mass-range extension techniques. With ESI, it is possible to measure a molecule that has a mass of 40,000 Da (if the molecule can hold 20 charges) since it will still have a m/z value of 2000.

The disadvantage of having multiple charges on a single molecule arises from isotopes.

Isotopes are heavy or light forms of the elements (i.e., containing a different number of neutrons) that comprise a molecule. For instance, most carbon atoms have a mass of 12 Da, but carbon also has a stable isotope with a mass of 13 Da that accounts for approximately 1.1% of all the carbon found in nature (Watson, 1985). Isotopes such as this do not pose a problem as singly-charged ions because the added mass shifts them to higher m/z values which can be resolved with the resolution available on commercial mass spectrometers.

With electrospray, however, isotopic ions that are 1 Da higher may now appear closer in mass-to-charge to the monoisotopic ions (whose mass is calculated using only the most abundant form of each element) because of the multiple charges. If an ion has an isotope 1 Da higher, but the ion has 2 charges, it will appear 0.5 m/z units higher than the monoisotopic mass. Figure 1-6 shows an example of human angiotensin I, $C_{62}H_{89}N_{17}O_{14}$, where this is true. As the number of charges increases, greater resolution is required if the mass spectrometer is to distinguish one isotope from another.

An interesting side-effect of isotopes is also visible in Figure 1-5. As the number of atoms in a molecule increases, the probability of that molecule containing isotopes of those atoms also increases. The peak at m/z 649.6 in Figure 1-5 is the monoisotopic peak (*M*) and, in this case, has a relative abundance of 100%. Since there are a large number of atoms in angiotensin I, the relative abundance of the isotope at m/z 650.1 (*M*+1) is rather large (~68%). If a molecule contains only atoms of carbon, hydrogen, nitrogen, oxygen, fluorine, phosphorus, and iodine, it is an easy task to calculate the approximate relative abundance of the *M*+1 and *M*+2 isotopes using the following equations (Silverstein et al., 1981):

$$\%(M+1) \approx (1.1 * \text{number of C atoms}) + (0.36 * \text{number of N atoms}) \qquad (1\text{-}9)$$

$$\%(M+2) \approx \frac{(1.1 * \text{number of C atoms})^2}{200} + (0.20 * \text{number of O atoms}) \qquad (1\text{-}10)$$

Ion Optics

Once the ions pass through the heated capillary, they undergo a jet expansion due to the reduced pressure on the exit side of the capillary. A tube lens helps to focus these expanding ions into a beam that is directed at an off-axis skimmer cone. The skimmer cone serves as a conductance limit and is positioned off-axis to prevent any solvated droplets from proceeding further toward the ion trap.

After the skimmer cone, two r.f.-only octopoles are used to transport the ions into the ion trap. The octopoles are separated by an inter-octopole lens that serves as an additional conductance limit as well as another means to remove any remaining solvated droplets. Normally, the octopoles are set to 400 $V_{p\text{-}p}$ with a frequency of ~2.45 MHz, but each octopole has a different DC offset. The second octopole should have a greater DC offset (i.e., more negative for positive ions) so that the ions are increasingly attracted toward the ion trap.

The LCQ Ion Trap

The LCQ ion trap is operated with a –10 V DC offset (for positive ions) applied to the entire trap, but with no DC potential between the ring and the endcap electrodes (i.e., U=0 in Equation 1-2). This means that all of the experiments done in an LCQ are performed along the a_z=0 line of the Mathieu stability diagram.

The trap itself does not conform to theoretical trap dimensions. It has an r_0=7.07 mm and a z_0=7.85 mm (Quarmby, 1997). This is a so-called "stretched trap" since the z_0 is greater than the ideal z_0 geometry (March and Hughes, 1989) of

$$z_0^2 = \frac{r_0^2}{2} \tag{1-11}$$

Based on the ideal geometry of Equation 1-9, the z_0 for a ring with r_0=7.07 mm would be 5.00 mm. Thus, a z_0 of 7.85 mm on the LCQ represents a significant stretch.

The stretched trap is necessary because perturbations in the quadrupolar field induce the superposition of higher order fields (Syka, 1995). These perturbations arise from truncated electrodes, the holes in the endcaps, and imperfect machining. It was discovered that the higher order fields caused some m/z assignments to be compound-dependent (Syka, 1995). Stretching the trap axially increased the amount of higher order fields, but improved the quadrupolar nature of the field in the center of the trap. It even led to improved resolution (Louris et al., 1992).

Ion Ejection

Ion ejection will be covered in detail in Chapter 3. Briefly, ions are normally ejected from the ion trap by ramping the amplitude of the main drive frequency on the ring electrode. This causes ions of successively increasing m/z to be ejected when they reach the β_z=1 line and enter into the region where they are axially unstable. When an ion becomes axially unstable, its maximum excursions from the center of the trap are greater than the size of the trap itself so the ion exits the trap through the holes in the endcaps or strikes the electrode. This ejection technique is called mass-selective instability (Stafford et al., 1984).

Alternatively, applying a supplemental AC voltage to the endcap electrodes to create an artificial stability boundary can eject ions. When the frequency of the supplemental AC matches the frequency of axial motion of the m/z of interest, the ion will absorb power from this resonant frequency and its axial displacement will increase until either it is ejected or it strikes an endcap. This technique is known as resonance ejection (Kaiser et al., 1991).

The LCQ uses mass-selective instability with resonance ejection to eject ions since the combination of the two gives better performance.

Ion Detection

When an ion leaves the trap through the exit endcap, it passes through a grounded exit lens (used to diminish fringing fields) and is attracted toward a –15 kV conversion dynode (+15 kV for negative ions) as shown in Figure 1-5. When the ions strike the surface of the conversion dynode, secondary particles are sputtered off of the dynode and detected and amplified by an electron multiplier (Schwartz et al., 1995). The current from the electron multiplier is sent to the electrometer circuit where the current is again amplified, converted to an analog voltage signal, and then converted to a digital signal. The digital signal is sent to the acquisition digital signal processor (DSP) which processes it and sends the signal to the data station where it is recorded as a mass spectrum.

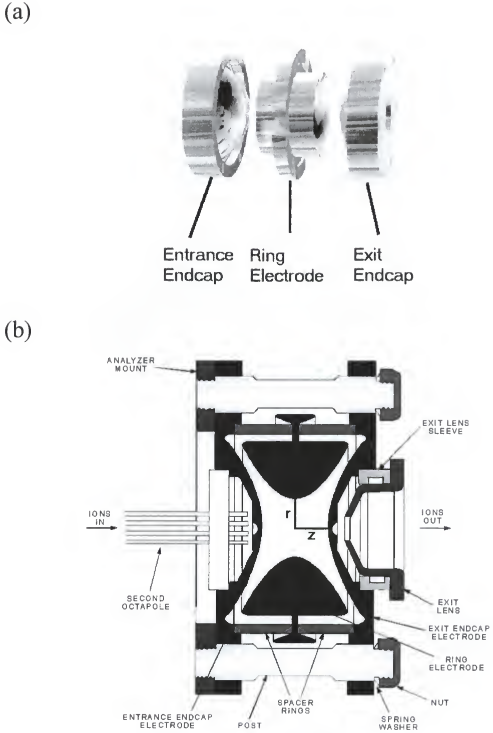

Figure 1-1. The quadrupole ion trap.

In (a), a typical set of ion trap electrodes is shown, while (b) is a cut-away view of the ion trap in the LCQ. Note that the radial and axial directions are labeled in (b) as r and z, respectively. Adapted from (DeGnore, 1996) (a) and the LCQ manual (LCQ, 1996) (b).

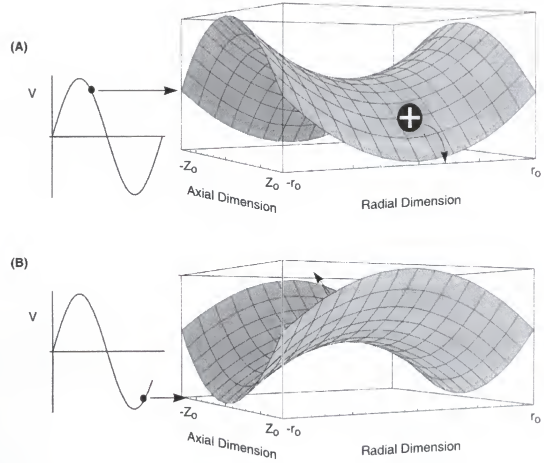

Figure 1-2. Changes in the trapping field due to the phase of the main r.f.

Changes in the potential of the main trapping field are shown as a function of the phase of the main r.f. denoted by the sine waves at left. In (A), the voltage on the ring electrode is in a positive phase and as a result, the positive ion is pushed toward either endcap (z_0 or $-z_0$). When the main r.f. goes negative (B), the situation is reversed and the ion is sent back toward the center of the trap to be attracted by the ring electrode (Wong and Cooks, 1997).

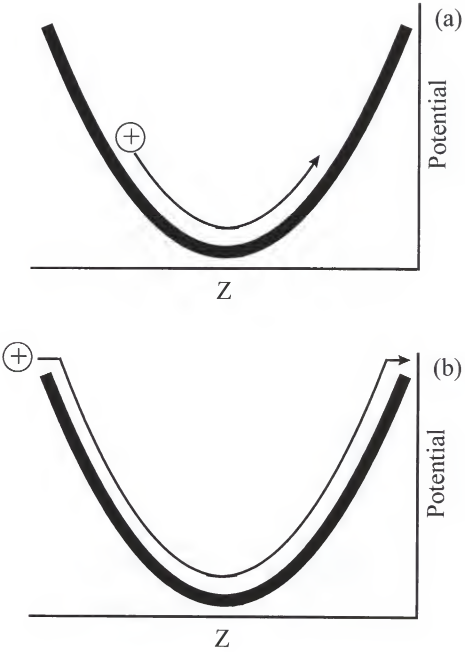

Figure 1-3. A representation of the psuedo-potential well.

An ion formed (a) inside the ion trap and (b) injected from outside the ion trap. The ion in (b) has enough kinetic energy to escape the potential well and to exit the trap. (Quarmby,1997)

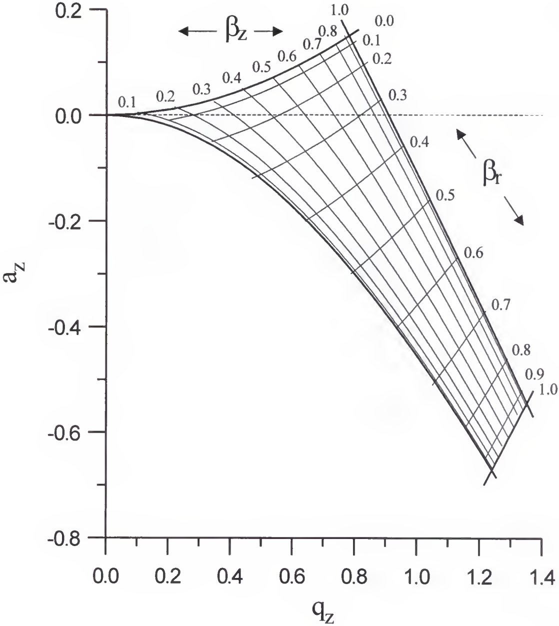

Figure 1-4. The Mathieu stability diagram.

The Mathieu stability diagram denotes the values of a and q that make an ion both axially and radially stable. The outer boundaries of the figure are defined by β_z=0 or 1, and β_r=0 or 1. The interior lines are intermediate values of β. Ions may have a and q values which make them stable in one dimension, but not the other. For instance, an ion at a_z= –0.4 and q_z=0.4 lies between β_r=0 and β_r=1 so it is radially stable, but it is not axially stable. To be axially stable, it must lie between β_z=0 and β_z=1.

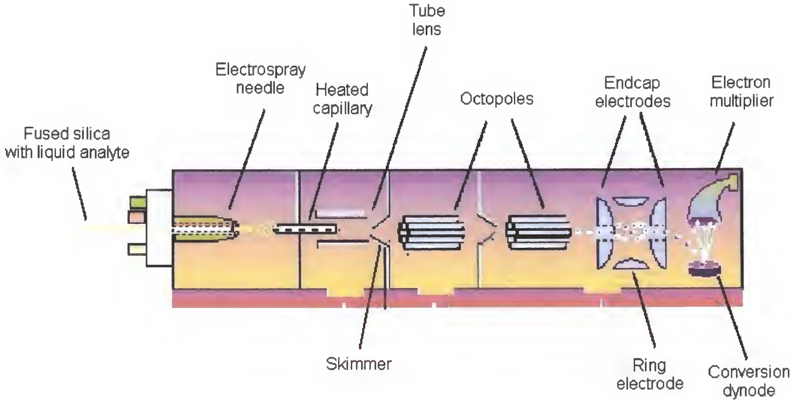

Figure 1-5. A diagram of the Finnigan MAT LCQ.

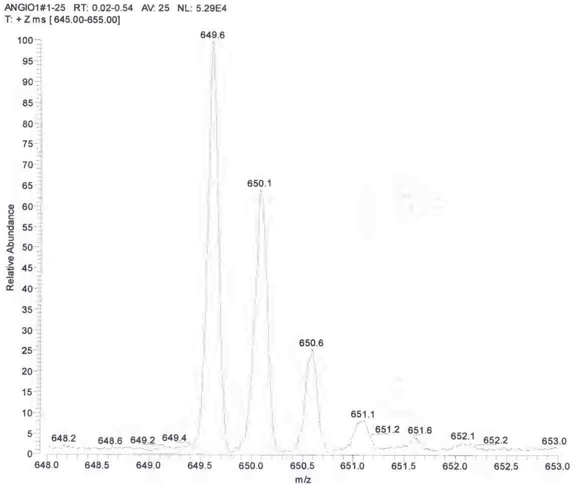

Figure 1-6. A mass spectrum of angiotensin I showing the +2 charge state (the $[M+2H]^{+2}$ ion).

This spectrum was obtained at high resolution so the isotopes can be seen every 0.5 m/z units. The peak at m/z 649.6 is the monoisotopic peak. The peak at m/z 650.1 is the result of ions containing a heavy isotope of one atom. The peak at m/z 650.6 is the result of ions containing two atoms the each have an extra neutron (e.g. two ^{13}C) and ions that contain one atom that has two extra neutrons (e.g. one ^{18}O instead of a ^{16}O).

CHAPTER 2
THE DEVELOPMENT OF MULTI-LEVEL CID AS AN ENHANCEMENT FOR MS^n ANALYSES

Introduction to MS/MS and MS^n

One of the inherent strengths of mass spectrometry has always been its ability to aid in the identification of unknowns by providing structural information through the mass analysis of fragment ions. The goal of coupling liquid chromatography (LC) to mass spectrometry (MS) was long pursued because LC/MS would be able to separate complex mixtures and provide clues to the identity of the mixture's components. Unfortunately, the ionization techniques that were ultimately successful in achieving this goal, such as electrospray and atmospheric pressure chemical ionization, are "soft" ionization techniques (Niessen and van der Greef, 1992) that form predominantly only a psuedo-molecular ion (providing only molecular weight information and no structural information).

Here, the benefits of a quadrupole ion trap become evident. The trap's ability to perform tandem mass spectrometry experiments (MS/MS and MS^n) that provide structural information through fragmentation of an ion of interest make it an excellent mass analyzer to mate to liquid chromatography (Creaser and Stygall, 1998). Using the trap's MS/MS ability, an ion can be isolated, excited, and dissociated by collisions so that its fragments (called daughter or product ions) can be mass analyzed to reveal structural information about the original isolated ion (known as a parent or precursor ion). With MS^n, one of the fragments from the MS/MS experiment may be isolated, excited and dissociated: thus, fragments of fragments may be mass analyzed so that the precursor ion's identity can be investigated piece by piece.

The Basics of Tandem MS on an Ion Trap

The first step in any LCQ experiment is ion injection. The ion trap is filled with numerous ions of various masses; the unwanted ions (those at mass-to-charge values different from the selected precursor ion) must be removed before the tandem phase of the experiment.

In order to remove unwanted ions from the trap, the fundamental principles of ion trap operation are applied. Remember that for a given r.f. voltage, ions of different masses will have different q values. Each q value corresponds to a β value that is related to the ion's frequency of motion in the ion trap by Equation 1-4. The LCQ brings the mass of interest (precursor ion) to q=0.83 and applies a tailored waveform (a sum of individual sine waves) which has frequency components that correspond to the frequencies of motion of all of the unwanted masses. Figure 2-1 shows a cartoon of a Fourier transform of this waveform as an example. The notch in the waveform is a range of frequencies around the frequency (ω_z) of the precursor ion. Since no voltage is being applied there, the precursor ion remains in the ion trap while the other ions are ejected. Note that the voltage is higher at the lower frequencies since the heavier masses reside there; it takes more voltage to eject an ion of higher mass.

The Excitation q

Once isolated, the mass of interest is dropped to a low q for excitation by reducing the amplitude of the main r.f. on the ring electrode. The q of excitation (q_{ex}) needs to be low since the product ions that are formed will be at lower m/z values, and thus higher q values. Since the goal is to mass analyze the product ions in a subsequent step, the q values of the product ions need to be less than 0.908 in order for those ions to remain stable in the trap. For example, if an ion of m/z 100 is excited at $q_{ex}=0.25$ (the default q_{ex} for the LCQ), and it forms product ions at m/z 80, 50, and 20, by Equation 1-7 the product ion at m/z 20 will not be stable in the trap (see below).

$$m_1 q_1 = m_2 q_2$$

$$100 * 0.25 = 20 * q_2$$

$$q_2 = \frac{100 * 0.25}{20} = 1.25, > 0.908$$

Of course, if observing the product ion at m/z 20 is important, the q of excitation can be lowered so that m/z 20 will remain in the trap. Dropping q_{ex} to 0.18 for m/z 100 means that m/z 20 will be at q=0.90. Unfortunately, the q of excitation needs to be a compromise between the mass range of the product ions and another aspect of the ion trap.

Psuedo-potential Well Depth

As mentioned previously, the ion trap often is considered to be a psuedo-potential well. Like any well, the pseudo-potential well has depth. Dehmelt approximated that the depth of the pseudo-potential well increased linearly with q (Dehmelt, 1967). Thus, lowering the q at which an ion in excited is equivalent to putting it in a shallower well. If the well becomes too shallow, the excitation may give the ion enough energy to escape the well before it fragments. In this case, no information is obtained.

Excitation

Once the precursor ion resides at the excitation q, the excitation needs to be applied. The frequency of the excitation is dependent on the choice of q_{ex} since q relates to β, and β relates to the frequency of ion motion, ω. In the LCQ, the excitation frequency is applied to the endcap electrodes in a dipolar fashion, meaning that each endcap has the same supplemental AC frequency, but the signals on the endcaps are 180° out of phase with each other. The supplemental AC is known as resonance excitation or axial modulation.

The amplitude of the resonance excitation is set by the user. The user selects a collision energy as a percentage (0-100%). In earlier versions of software, 100% collision energy was equivalent to a 5 V_{pp} excitation. In the Xcalibur software, a new algorithm for determining the excitation voltage from the percent collision energy was implemented. This algorithm, known as normalized collision energy (Lopez et al., 1999), is a linear function of the m/z of the precursor ion as well as the percent collision energy entered by the user. The slope and intercept of this line change when the instrument is calibrated. Normalized collision energy will be discussed in more detail later in the chapter.

Mass Analysis

Once the excitation frequency has been applied, the only remaining step is to mass analyze the product ions that may have been formed. The mass analysis (sometimes called a scan-out) is a typical LCQ mass analysis. Ions are ejected through the exit endcap and detected with the conversion dynode and electron multiplier.

Problems with LC/MS^n Analyses

The problem with MS^n analyses arises when they must be performed on a time-varying sample, such as compounds eluting from an LC column. When a complex mixture of components is being separated, each component is flowing into the mass spectrometer to be analyzed using MS^n. The mass spectrometer is either pre-programmed with specific masses to fragment, or the software can dynamically choose which mass to use for the tandem experiment (LCQ, 1996). In either case, there is a finite time (on the order of seconds) that any particular component will be flowing into the mass spectrometer. There is not enough time to optimize the collision energy to use for each compound during the tandem experiments, and a single selected collision energy may not be effective for all compounds. Generally, each component will have only a limited range of collision energies that will bring about fragmentation.

Figure 2-2 shows the collision energy curve for caffeine's $[M+H]^+$ ion (m/z 195) obtained during an infusion experiment. It is clear from the narrow range of collision energies that generate the dominant product ion m/z 138 that setting an appropriate collision energy is a tricky task. Too much collision energy (excitation voltage) ejects the precursor ion prior to fragmentation, resulting in a blank, noise-filled mass spectrum. Not enough collision energy is insufficient to cause fragmentation so the only mass that appears in the mass spectrum is the uninformative precursor ion.

Even seemingly small changes to an ion can impact the range of effective collision energies. For example, the $[M+H]^+$ and $[M+Na]^+$ ions of erythromycin shown in Figure 2-3 have distinctly different optima. In the case of the $[M+H]^+$ ion, a collision energy of 20% is the optimum for the two primary product ions, while 20% collision energy does not even have begin to fragment the $[M+Na]^+$ ion.

It is clear that collision energies need to be optimized for parameters such as mass, charge, and ion type. In an LC run, a compromise collision energy would result in missed information from components for which the precursor ions are either ejected or do not fragment. To obtain this information, the analysis would have to be repeated using alternate collision energies.

The Development of Multi-level CID

Nathan Yates, a graduate from the University of Florida under Dr. Yost, had an original idea that could avoid the need to repeat LC/MS^n analyses at different collision energies and improve the efficiency of MS^n. Since there is not enough time to optimize collision energy during the elution of an LC peak, his idea was to subject the parent ion to three separate collision energies before the product ions are scanned out for mass analysis. The implementation of this idea relies on the physics of the ion trap. The collision energies would have to be applied in increasing order to greatly improve the opportunity for producing fragment ions before losing the parent ion due to ejection. If the collision energies were decreased, the parent ion may be subjected to too much collision energy in the first CID event, resulting in ejection; thus, no parent ion would be left in the trap to excite in the following CID events.

From the product ions' point of view, the added collision energies are of no concern. The precursor ion is being excited at q_{ex} with a specific frequency, ω_z. If the product ions are formed in the first CID event, the second and third are of no consequence since the product ions fall at different q values, have different frequencies, and thus, are not being excited. In effect, the product ions cool until they are subjected to mass analysis.

With regards to the LC, adding additional CID events would add only tens of milliseconds to a scan. Since LC peaks are typically a few seconds wide, the added CID time minimally impacts the number of scans that could be generated to define the peak.

With this idea in hand, work was begun on what was dubbed "multi-level CID."

Preliminary Work

Figure 2-4 compares a typical scan function for multi-level CID with one for normal CID. The amplitude of the main r.f. on the ring electrode is represented by a digital-to-analog converter (DAC) value which is proportional to q (higher DAC means higher q). The resonance excitation trace represents the voltage on the endcaps during a scan. The injection, isolation, and mass analysis events are identical in both scan functions; only the CID events differ due to the addition of two 30 ms excitation events of successively increasing voltage. By comparing the overall time of each scan function, it is apparent that the addition of the extra events to multi-level CID is not a significant time penalty.

Determining Additional CID Voltages

For the preliminary work, a simple set of coefficients was applied to the collision energy entered by the user in order to assign the voltages for the additional resonance excitation events. The choice of coefficients for the three levels was simple. For the first level of CID, 1/3 of the user-entered collision energy was applied. For the second level, 2/3 of the user-entered collision energy was applied. Finally, all (3/3) of the user-entered collision energy was used to excite the parent ion.

Figure 2-5 shows a comparison of collision energy curves for the $[M+H]^+$ ion of benzamide using normal CID and multi-level CID. It is important to note that each collision energy value shown on the *x*-axis for the multi-level CID actually represents three collision energies due to the three steps. The collision energy being plotted is the percentage entered by the user, which is multiplied by 0.33, 0.67, and 1 to generate the three levels. Thus, the product ion intensity at a value of 30% in multi-level CID should be approximately equivalent to the sum of the intensities at 10, 20, and 30% using normal CID.

It is clear from Figure 2-5 that there is substantial improvement in the range of acceptable collision energy choices. Without multi-level CID, any percentage above 20 resulted in an essentially blank mass spectrum. With multi-level CID, choices as high as 40 percent resulted in an acceptable MS/MS spectrum.

As more compounds were tested using multi-level CID, it was evident that the coefficients that were chosen were very effective for small molecules, but ineffective for heavier compounds that require a great deal of collision energy to cause fragmentation. For example, Figure 2-6 shows the collision energy curves for $[M+Na]^+$ of gramicidin A (m/z 1903) and two of its most abundant fragment ions using single-level and multi-level CID. Recall that coefficients less than one expanded the acceptable range of collision energies to higher percentages. Gramicidin A is an example where expanding to higher percentages is ineffective. Expanding the range of collision energies for gramicidin A requires coefficients higher than one so that efficient CID is observed even when the user specifies a low percentage.

Since there was already a growing database of collision energy curves using 0.33, 0.67, and 1.0 as coefficients, and a great deal of success was achieved using these values, it was deemed that multi-level CID should be expanded to four levels with the last level having a coefficient of 1.5.

Figure 2-7 demonstrates the effect that adding the fourth level had on the gramicidin S collision energy curve. Now, collision energies from 38 to 60% gave high intensity fragment ions, whereas almost no intensity was obtained at these requested collision energies previously. An important feature of Figure 2-7 is the valley in the intensity of the product ions that appears when collision energies around 60% are chosen. This bimodal distribution of product ion intensity was a recurring feature on almost all of the compounds tested using multi-level CID; though the valley would appear at different percentages for different compounds (see Figure 2-5 at 20% collision energy).

Obviously, it would be beneficial to have an almost constant response from product ion intensity across the range of acceptable collision energies rather than some values being better than other values. However, it is important to note that a satisfactory MS/MS spectrum is still obtained even if the collision energy is set to the point of the valley. An attempt was made to achieve more consistent intensities by changing the coefficients used to calculate the resonance excitation voltage.

Figure 2-8 shows the resulting collision energy curve when the second level coefficient is changed from 0.67 to 0.5 for the $[M+H]^+$ of benzamide. Despite a narrow drop in intensity around 17%, the bimodal nature of the previous collision energy curve is almost eliminated. This result spurred an attempt to mathematically model the collision energy coefficients needed to generate a more constant product ion intensity.

Modeling Multi-level CID Behavior Mathematically

The $[M+H]^+$ ion of caffeine was chosen as the model because it formed only one dominant product ion and the range of collision energies that was capable of producing fragmentation was among the narrowest of any of the compounds tested.

An fifth-order polynomial curve which mimicked the intensity profile of caffeine's product ion at m/z 138 was used to generate theoretical collision energy curves for multi-level CID using various coefficients. Figure 2-9 is a comparison of the mathematical projection of having four levels of CID with coefficients of 0.33, 0.5, 1.0, and 1.5 to the actual data collected using these four levels. It is clear that the model did an excellent job of predicting the intensity profile that was obtained. The valleys which were predicted at 13, 22, and 35% were all present in the actual data, and the depths and widths of these valleys were in good agreement with the prediction.

For a short time, a fifth level of CID was investigated, but it became clear from the mathematical model that more coefficients would have to be implemented if multi-level CID was going to provide a flat product ion intensity profile over a wide range of collision energies. As a test case, multi-level CID was expanded to ten levels with coefficients that were determined using the model. The $[M+H]^+$ ion of caffeine was subjected to this 10-level CID with coefficients of 0.17, 0.20, 0.25, 0.33, 0.40, 0.50, 0.67, 1.0, 1.5, and 2.2. Since 10 levels would begin to add a significant cost in time to the scan, the excitation time was varied from 10 to 30 ms per level of CID to see if shorter times could be used. It was discovered that 20 ms per level of CID gave almost equivalent intensity to 30 ms per level. Figure 2-10 displays the comparison of the projected curve with its real data counterpart for ten-level CID using 20 ms per level. A very flat intensity profile was achieved with 95% coverage of collision energy choices; only selections below 5% gave no product ions.

Automating Multi-level CID

Even with the reduced excitation time, 200 ms for CID per microscan seemed to be too long since typically three microscans are averaged before data is sent to the data station (an analytical scan). In this case, 10 levels of CID would add over a 0.5 s to an analytical scan, and that would significantly impact the number of points per LC peak that would be recorded. Additionally, much of that time is wasted since the fragmentation probably occurs on only one or two levels. Once all of the parent ions are fragmented and/or ejected, there is no point in applying higher excitation voltages, but there is no way of knowing which levels are not needed.

It was therefore deemed necessary to devise a way of automating the multi-level CID process. If a way could be found to spend more time on collision energies which were capable of causing fragmentation (and virtually no time spent on energies that would cause precursor ion ejection), then fewer levels of CID would be needed and the scan could be shortened.

Personal experience and private communication (Jodie Johnson and Jae Schwartz) suggested that the primary parameter for determining an appropriate collision energy was the precursor ion's mass-to-charge ratio. The higher the m/z, the higher the collision energy needed to be to produce fragmentation. Assigning a maximum voltage as a function of mass-to-charge would be a good way of forcing multi-level CID to spend more time on effective collision energies. The problem was determining that function.

As mentioned previously, the parameter q determines the depth of the psuedo-potential well. Dehmelt (1967) proposed an expression (given below) for the depth of the well, D_z, which has been verified experimentally for $q_z<0.4$ (Fulford and March, 1979).

$$\overline{D}_z = q_z \frac{V}{8} \tag{2-1}$$

From this expression, the depth of the well is linearly related to q_z. The LCQ uses a linear calibration for the resonance ejection voltage (V_{ej}) as a function of mass-to-charge ratio. Since this is the voltage necessary to cause ion ejection at the ejection q, q_{ej}, it would be a simple matter to determine the ejection voltage for any particular m/z at any excitation q by a simple formula:

$$V_{ex,max} = \frac{q_{ex}}{q_{ej}} V_{ej}$$

(2-2)

This relationship was incorporated in multi-level CID so that the user-entered collision energy could be removed. With a maximum voltage defined as the last level of CID, it was now possible to determine how many levels of CID would be necessary as well as how long should be spent on each level.

Parameters for Automated Multi-level CID

The coefficients for each level of CID were changed so that they increased by $1/n^{th}$ where n is the number of levels of CID. For instance, if five levels of CID were used, the coefficients would be 0.2, 0.4, 0.6, 0.8, and 1.0. These coefficients would be applied to the maximum voltage that was calculated by equation 2-2.

Experiments were run on various compounds to investigate how many levels of CID would be necessary and how much time should be spent on each level. The number of levels of CID was varied from 1 to 20. Additionally, 10 ms, 20 ms, and 30 ms of excitation per level were also investigated. Figure 2-11 shows the results of one of these experiments for the primary product ion of the $[M+H]^+$ of benzimidazole. One level of CID produced only minimal fragmentation since it was using the maximum voltage calculated from equation 2-2. In this case, most of the precursor ions were probably ejected before much fragmentation could occur. Two levels of CID did not provide much benefit since the range of acceptable collision energies was narrow and even half of the maximum voltage is probably still too much. When three levels of CID were used, a dramatic increase is product ion intensity is evident. Except for the dip in intensity at four levels, there is an essentially flat response after three levels of CID. Other compounds showed similar behavior, but sometimes the dramatic increase in intensity and subsequent leveling off did not occur until levels four or five. It was therefore determined that five levels was would be the best number to use for future experiments.

As a test for automated multi-level CID, an LC/MS/MS analysis of polyethylene glycol (PEG) 600 was performed. A gradient elution on a 4.6 mm i.d. C8 column was used to separate the various chain lengths of polymers in PEG 600 with the following conditions:

A: 1% Acetic Acid

B: Acetonitrile

Gradient: 15–35% B in 25 mins. @ 1 mL/min.

The PEGs eluted in order of increasing monomer units as $[M+NH_4]^+$ ions (not $[M+H]^+$ ions, probably due to contamination of the sample). For the multi-level CID analysis, five levels of CID were used with 20 ms of excitation per level. For comparison, the assay was re-run using 20, 50 and 80% collision energy values by conventional single-level CID. Figure 2-12 is the chromatogram obtained from the multi-level CID run. The peaks are labeled in three ways:

1) The m/z of the $[M+NH_4]^+$ ion of PEG in the full scan mass spectrum is given.
2) Successful MS/MS spectra obtained using 20% collision energy are denoted with stars.
3) Successful MS/MS spectra obtained using multi-level CID are denoted with happy faces.

Qualitatively, it is clear that multi-level CID more successfully fragmented the PEGs over a wider m/z range.

To provide a quantitative analysis, the CID efficiency of each analysis was calculated. CID efficiency is calculated by the equation

$$Efficiency(\%) = \frac{\Sigma F_i}{P_0} \times 100 \qquad (2\text{-}3)$$

where ΣF_i is the sum of the fragment ions intensities obtained from MS/MS and P_0 is the intensity of the precursor ion obtained without fragmentation. In order to do this calculation, the LC analysis was run using both single-level and multi-level CID without any collision energy so that P_0 for each method could be obtained.

Figure 2-13 is the resulting CID efficiency plot for several of the PEGs. Multi-level CID has the overall best efficiency. Though 20% collision energy is better at some of the lower m/z values, its effectiveness falls off rapidly as the mass-to-charge ratio increases. Using 50% collision energy did provide fragmentation data for all of the PEGs, but it is clear from the efficiency plot that the intensity of the product ions is not very good compared to multi-level CID. Eighty percent collision energy did not provide much information since it was causing more ejection than fragmentation of the precursor ions.

A False Premise

Despite the fact that automated multi-level CID was working well, there was a flaw in the premise of calculating a maximum voltage using a ratio of the excitation q to the ejection q. The problem arises because Dehmelt's approximation for well depth is only appropriate for $q_z<0.4$ and the ejection q for the LCQ is 0.9. Simulations of well depth at higher q values (Pedder, 1992) showed that the well depth increases up to a q of approximately 0.7 and then rolls over and decreases dramatically as $q_z=0.908$ is approached (see Figure 2-14). Therefore, the voltage that would cause ejection at the excitation q may be almost the same as the voltage that would cause ejection at the ejection q. This meant that the maximum voltage chosen for multi-level CID may not work for all compounds.

In order to remedy this situation, an experimental study of well depth at q values greater than 0.4 was undertaken since no previous work could be found in the literature. This study involved what has sometimes been referred to as a "survivor ion" scan. The scan consists of normal events such as injection and isolation, but then is divided into two main events. The first event consisted of an almost normal LCQ ejection, but the supplementary AC signal is applied at the q of interest. The amplitude of this ejection frequency is initially set to zero, but is ramped up in successive scans. The second event is a normal scan-out event at q_{ej}=0.9. Since the amplitude of the supplemental AC frequency was set to zero initially during the first ejection event, the scan-out at q_{ej}=0.9 provides information on the intensity of the ions when they have not been perturbed at all at the q of interest. As the amplitude of the ejection frequency is increased in the first event, the intensity of the ions during the later scan-out event diminishes since some of the ions have been ejected at the q of interest. Plotting the intensity of the precursor ion as a function of the ejection amplitude gives a "reverse" s-curve that provides information on how many ions have survived being ejected during the first event. The ejection voltage at which the intensity of the precursor ion reaches zero reveals the point at which there are no survivors since all of the ions were ejected during the first event.

Figure 2-15 shows some typical reverse s-curves for the $[M+H]^+$ ion of benzimidizole at different q values of interest. Since the point at which the intensity reaches zero is difficult to judge for different q's, the more easily distinguishable point half-way between full precursor ion intensity and zero precursor ion intensity was used to assign well depth for subsequent plots.

Figure 2-16 is the well-depth curve that is generated by plotting the 50% survivor voltage for benzimidizole ejection over a range of q values. It is clear from the plot that the simulations of well depth are correct and that there is a substantial decrease in the depth once q_z=0.7 is passed.

Problems with Well depth

Unfortunately, the data from Figure 2-16 are not immediately applicable to assigning a new maximum voltage for multi-level CID. The data in Figure 2-16 were collected using an ejection process at each of the various q values. CID is an excitation process, which requires lower voltages applied over a longer period of time.

In the LCQ, ejection is done by applying a fixed resonance ejection frequency on the endcap electrodes which has sufficient voltage to cause ejection of the ions as they are pushed towards this frequency by the ramping of the main r.f. amplitude on the ring electrode. Excitation in the LCQ, however, is a two-step process where the ions are pushed through the resonance excitation frequency and then pulled back through that frequency by increasing and then decreasing the amplitude of the main r.f. on the ring electrode. Therefore, it was necessary to duplicate the well-depth data from Figure 2-16 using an excitation, and not an ejection, event.

Figure 2-17 shows the well-depth data for the [M+H]+ ion of benzimidazole obtained using an excitation event. It is evident that there is a substantial shift in the well-depth maximum from the previous data. The problem with the well-depth plots using the excitation event is that some of the reduction in intensity obtained in a survivor ion curve may be due to fragmentation, not just ejection. While an effort was made to choose compounds that did not fragment under typical CID conditions, even these compounds showed product ions as the q of excitation was increased. Additionally, the change in intensity that is due to fragmentation is difficult to account for since the product ion m/z range is changing for each q investigated.

Keeping in mind that the ultimate goal of the well-depth study was to determine a relationship between the maximum voltage for use in multi-level CID and mass-to-charge, an alternative to studying small organic molecules was found.

To alleviate the problem of possible fragmentation, some elemental ions were investigated. Iodide and bromide were electrosprayed as cesium salts. This was the first look at well depth with negative ions. An interesting feature developed from the well-depth analysis of these halide ions. For some reason, there was a dip in the well depth around q_z=0.3, as can be seen in Figure 2-18. This dip was verified experimentally on several occasions. According to Dehmelt's approximation, which to this point had held true for all of the compounds tested, the well depth should continue to increase linearly until q_z=0.4. These unusual dips were unexpected and unexplainable.

As a check, the well depth of the positive elemental ion, cesium, was profiled. There was no dip. Since finding the cause of these aberrations in the well depth of bromide and iodide could be a research project unto itself, the investigation of elemental ions was shelved. Additionally, it was clear that there were not enough elemental ions that could be electrosprayed to cover the mass range that multi-level CID would have to cover when determining its maximum voltage.

A New Solution

In June of 1999, Jen Gidden presented a talk at the American Society for Mass Spectrometry conference about the stability of sodiated PEG ions (Gidden, 1999). Due to the floppy nature of PEG ions and the alternating electronegative oxygens, PEG wraps itself around a sodium ion to form a very stable structure similar to crown ether. Some chain lengths of PEG are more stable than others, but overall this is a very stable complex.

A second look at my earlier PEG work with multi-level CID revealed that sodiated PEG ions ($[M+Na]^+$) were intermingled with the $[M+NH_4]^+$ ions in each of the LC peaks. Close inspection of the MS/MS spectra for the sodiated PEG peaks revealed one of two cases: either no fragmentation at all, just an isolated parent ion with a very clean baseline; or a completely blank spectrum. Apparently, the sodiated PEGs were so stable that they were not fragmenting, but they were ejecting when very high collision energies were used. This revelation provided an excellent means of determining the maximum voltage to use for multi-level CID as a function of mass-to-charge since the sodiated PEG ions were so stable that only ejection was observed. Additionally, PEG ions vary in mass by only 44 Da and cover a wide mass range.

A shortened well-depth study which focused on typical excitation q values was initiated using various $[M+Na]^+$ ions for PEG 600. Ions from m/z 481 to m/z 877 were investigated as well as q_{ex} of 0.20, 0.25, 0.35, 0.40, 0.45, though not all ions were investigated at all q values. Figure 2-19 is a combined plot of the various ions and q values. Each q_{ex} shows a linear relationship between the voltage required to eject 50% of the precursor ions and the m/z of that ion. In fact, all of the data show a similar slope and intercept regardless of the excitation q, with the exception of q_{ex}=0.20. The slope for the data at q_{ex}=0.20 was nearly 10–20% greater than the other data. With this in mind, all of the data except q_{ex}=0.20 were combined and an overall equation relating the 50% ejection voltage to the mass-to-charge was determined. Figure 2-20 shows this line and its equation.

The equation to the line in Figure 2-20 was implemented in the multi-level CID scan function with one minor change. Since the equation was determined by the ejection of only 50% of the precursor ions, the intercept was adjusted upwards by 0.2 V so that nearly all of the ions would be ejected on the last level of CID if they had not fragmented on earlier levels. This adjustment helps to guarantee that if an ion will fragment in the ion trap, it will be given enough voltage to do so using multi-level CID.

Final Testing of Multi-level CID

With the completion of the maximum voltage calculation, testing was initiated on multi-level CID with Nathan Yates at Merck & Co., Inc. in Rahway, NJ. While there, a comparison between fixed collision energy, normalized collision energy, and multi-level CID was performed on a tryptic digest of the protein myoglobin.

Normalized Collision Energy

Normalized collision energy (NCE) is the term used to describe a new algorithm for determing the amplitude of resonance excitation that was developed by Jae Schwartz of Finnigan (Lopez et al., 1999). Basically, it takes a user-specified collision energy percentage and scales the amplitude of resonance excitation linearly with mass-to-charge. The slope and intercept of the mass-to-charge adjustment are determined during instrument calibration. The resonance excitation amplitude (V_{ex}) is calculated by the following equation:

$$V_{ex} = \left(\frac{CE\%}{30}\right) * \left[\left(\frac{m}{z} * slope\right) + intercept\right] \tag{2-3}$$

where *CE%* is the user-specified collision energy percentage, *m/z* is the mass-to-charge of the precursor ion selected for fragmentation, and the *slope* and *intercept* are calibrated parameters (typically 0.001 and 0.4, respectively). Note that the user-specified collision energy still has a significant role in determining the final voltage of excitation. Entering a value of 60% gives twice as much voltage as 30% across the entire mass range.

Comparison of CID Techniques

A tryptic digest of myoglobin was performed in order to break the large protein down into a large number small peptides that could be easily chromatographed using micro-LC. The micro-LC columns were loaded with the digested sample using a pressurized bomb, and as such, the injection volumes were not accurately known. Despite this fact, every attempt was made to perform reproducible injections.

A separate data-dependent LC/MS/MS run was performed using each of the CID techniques where the MS/MS scan would be triggered on the tallest mass-to-charge peak from a full scan mass spectrum. There was a fixed (35%) collision energy run and two normalized collision energy runs, one at 30% and the other at 35% collision energy. The multi-level CID run was also performed, without specifying any collision energy.

Figure 2-21 shows the results from each of the CID techniques for m/z 748.4 (peptide ALELFR). The fixed collision energy spectrum (a), in which 1.75 V_{pp} excitation was applied to all ions, show a significant number of product ions and no precursor ion remaining. The 30% NCE spectrum (b) has almost no product ions at all. The only intense ions present in the spectrum are the precursor ions, resulting in a completely uninformative MS/MS spectrum. Amazingly, the 35% NCE spectrum (c) contains a substantial amount of product ions, with some parent ions remaining around m/z 749. The multi-level CID spectrum (d) shows a similar amount of product ions, but no parent ion at all.

Another example of a myoglobin peptide identified for MS/MS is given in Figure 2-22. The peptide HGTVVLTALGGILK (m/z 1378.7) was subjected to the 1.75 V_{pp}

excitation in the fixed collision energy LC/MS/MS run (a). Unlike the former case with m/z 748.4, m/z 1378.7 did not fragment at all. This excitation voltage was too small to fragment a peptide nearly twice the mass of the earlier one. Likewise, the 30% NCE run (b) had trouble fragmenting this peptide, but did provide a few low intensity product ions. At 35% normalized collision energy (c), m/z 1378.7 is completely gone and a rich product ion spectrum remains. Multi-level CID (d) shows almost an exact match to the 35% NCE spectrum.

Conclusions for Multi-level CID

Figures 2-21 and 2-22 are just two examples from the numerous peptides that were selected for MS/MS in the myoglobin digest sample. Many of the spectra appeared similar for all four LC/MS/MS runs. In fact, multi-level CID and 35% NCE were almost identical in every case. However, Figure 2-21 reveals the major weakness of normalized collision energy; that is, it still requires the user to specify the collision energy. A small change of only 5% in the user-specified collision energy took the resulting spectrum from completely uninformative to useful. It is easy to see how a user could select a collision energy that is just slightly outside the acceptable range and have to re-run their experiment at a different collision energy. Multi-level CID eliminates that possibility.

In terms of sensitivity, multi-level CID and 35% NCE seemed approximately equivalent. Both techniques tended to completely eliminate the precursor ion from their MS/MS spectra, indicating an efficient conversion of parent ion to product ion. However, at higher collision energy percentages this may not be the case.

Overall, normalized collision energy is a strong improvement over fixed collision energy. Multi-level CID has the potential to be a stong improvement over normalized collision energy, but more study will have to be conducted to determine the ultimate strengths and weaknesses of each technique.

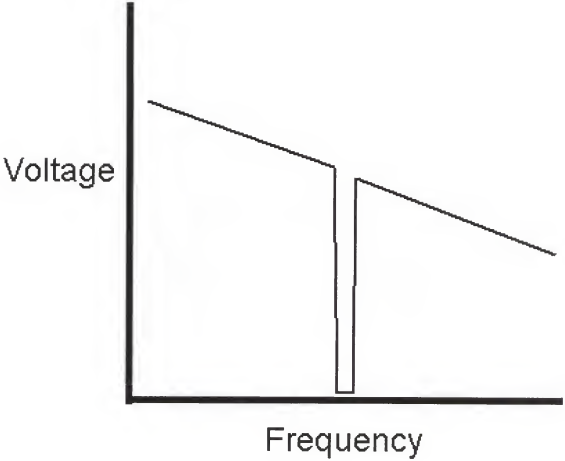

Figure 2-1. A cartoon of a Fourier transformation of the isolation waveform of the LCQ.

The figure shows the notch for isolation and the decreasing voltage at higher frequencies (ions of low m/z reside at high frequency and require less voltage for ejection.)

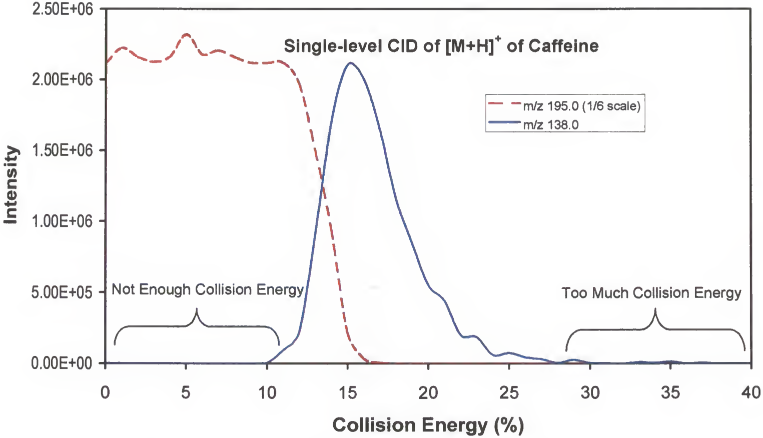

Figure 2-2. A collision energy curve for the $[M+H]^+$ ion of caffeine.

The intensity of the [M+H]+ ion of caffeine at m/z 195 and its primary fragment ion at m/z 138 are shown as a function of collision energy. The intensity of the product ion at m/z 138 demonstrates the narrow range of collision energies that successfully fragment caffeine.

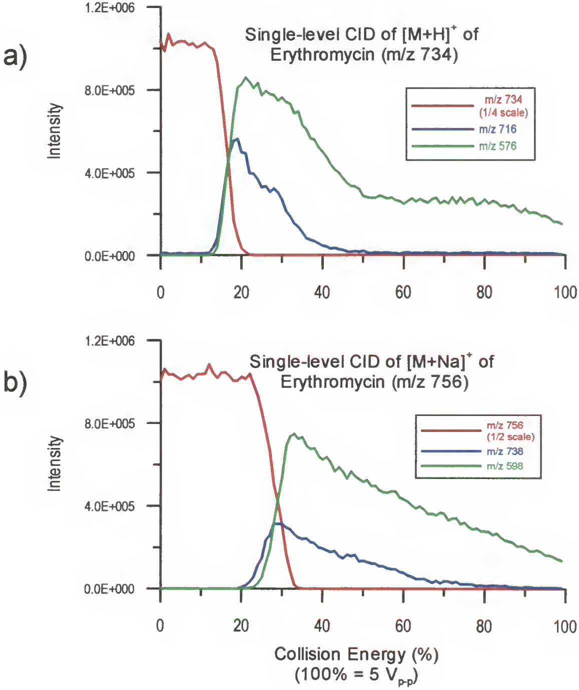

Figure 2-3. Collision energy curves for $[M+H]^+$ and $[M+Na]^+$ ions of erythromycin.

A comparison between the $[M+H]^+$ (a) and the $[M+Na]^+$ ion (b) of erythromycin. Note difference in the optimum collision energy for each ion.

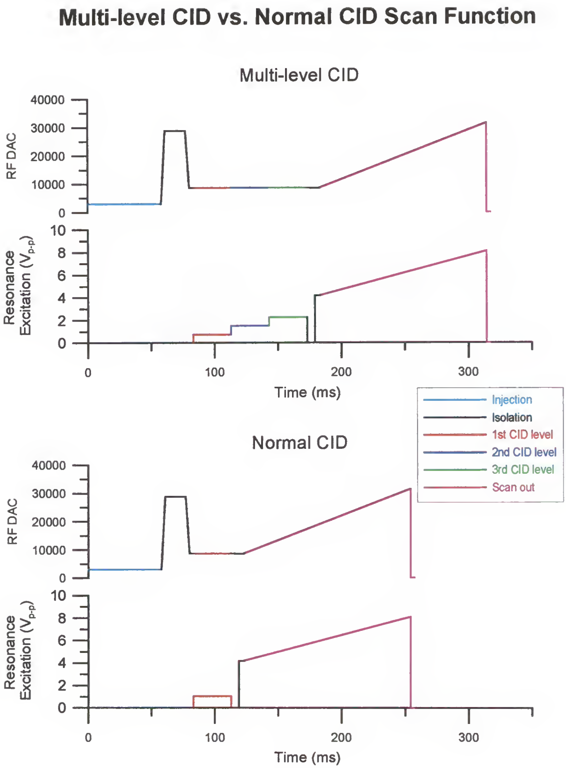

Figure 2-4. Scan function plots for multi-level and single-level CID.

A comparison of the multi-level CID scan function with a normal single-level CID scan function. The RF DAC plots represent the voltage on the ring electrode, while the resonance excitation plots represent the voltage on the endcap electrodes.

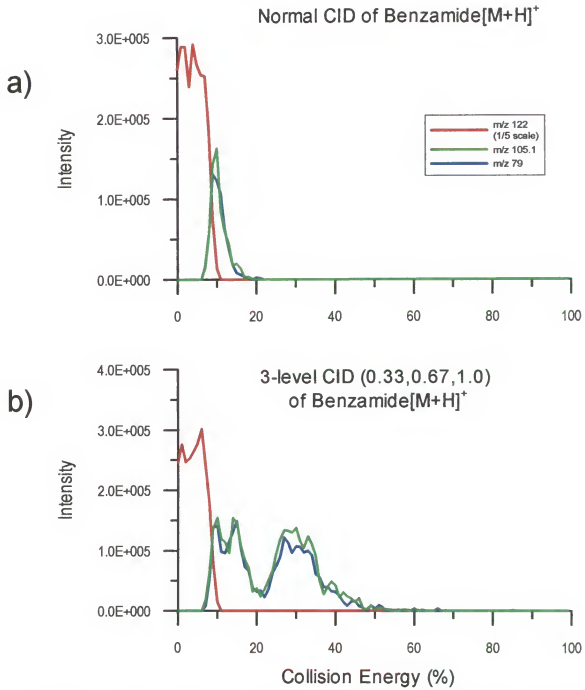

Normal CID of Benzamide$[M+H]^+$

3-level CID (0.33,0.67,1.0) of Benzamide$[M+H]^+$

Figure 2-5. Collision energy curve for the $[M+H]^+$ ion of benzamide using single-level and multi-level CID.

A comparison of single-level CID (a) with multi-level CID (b) on the $[M+H]^+$ of benzamide. Note the extension of acceptable collision energies using 3 levels of CID.

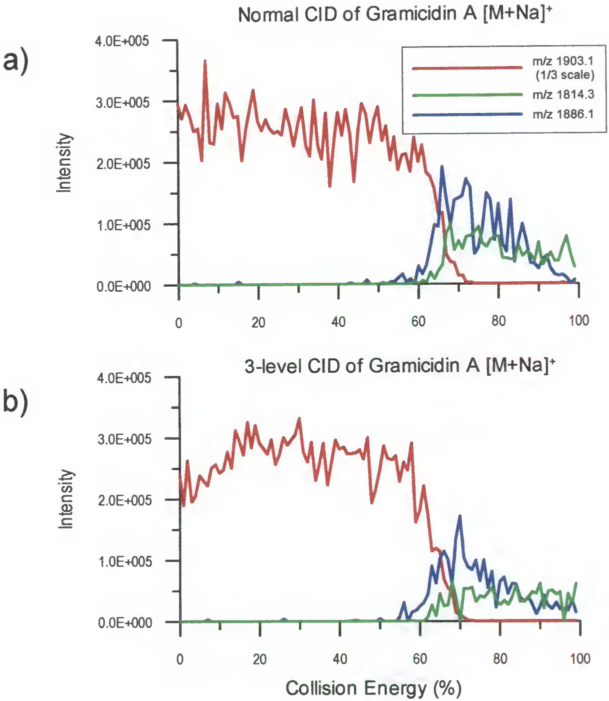

Figure 2-6. Single-level and multi-level CID of the $[M+Na]^+$ of gramicidin A

The coefficients of 0.33, 0.50, and 1.0 are ineffective for multi-level CID in this case.

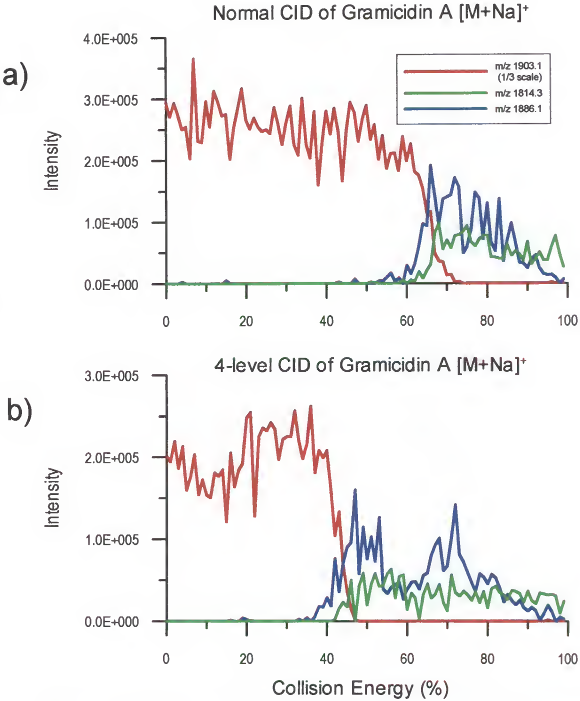

Figure 2-7. Collision energy curves for the $[M+H]^+$ ion of gramicidin A with a fourth level of CID.

Adding a fourth coefficient of 1.5 has expanded the range of collision energies for gramicidin A where three levels were ineffective.

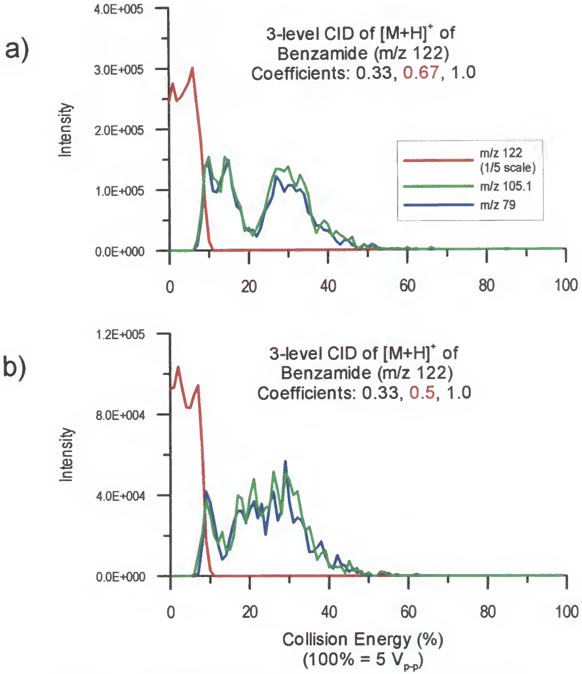

Figure 2-8. The effects of changing the second multi-level CID coefficient.

Note the disappearance of the valley at 20% collision energy by changing the second coefficient from 0.67 (a) to 0.5 (b).

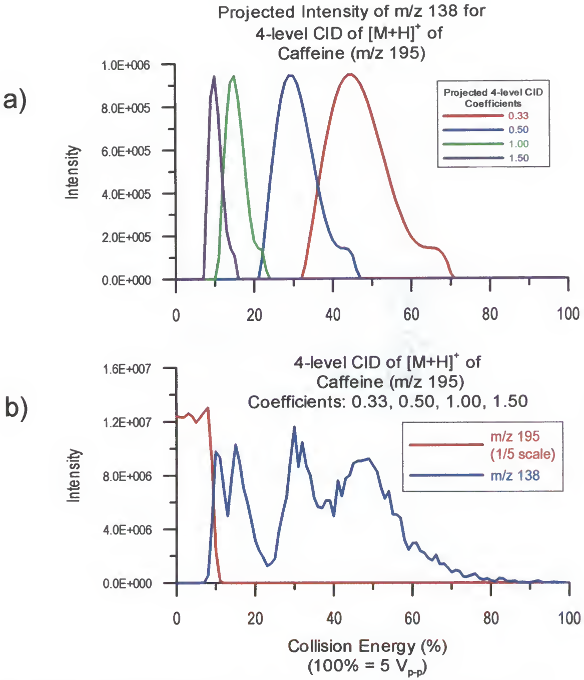

Figure 2-9. A comparison of predicted and actual collision energy curves for caffeine using four-level CID.

The mathematical projection of a 4-level CID collision energy curve of caffeine is given (a). The corresponding actual data (b) match very well with the prediction.

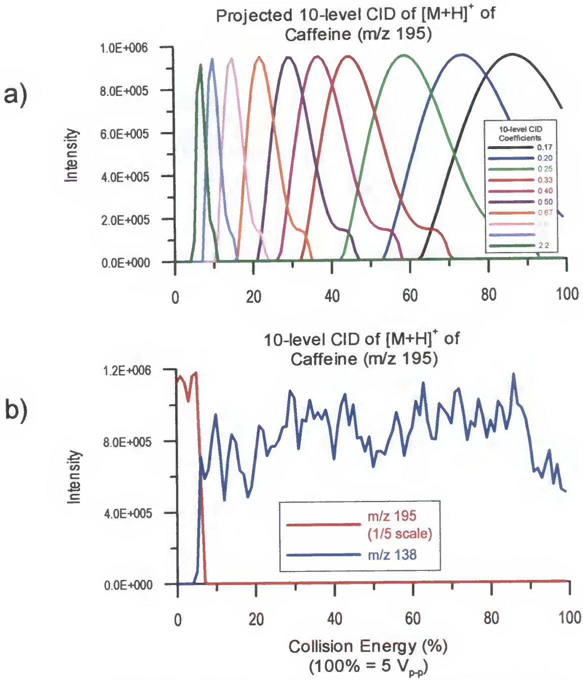

Figure 2-10. A comparison of predicted and actual collision energy curves for caffeine using ten levels of CID.

The mathematically predicted curve for 10 levels of CID of caffeine (a) is compared to the actual data generated using the predicted coefficients (b).

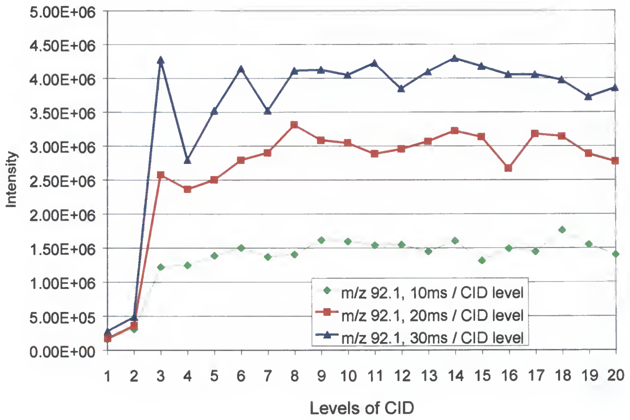

Figure 2-11. Intensity of product ion as a function of the number of CID levels.

The intensity for product ion m/z 92 of benzimidazole is plotted as a function of the number of levels of CID. Note the dramatic increase in product ion intensity when 3 levels of CID are used and the subsequent leveling off of intensity with more levels.

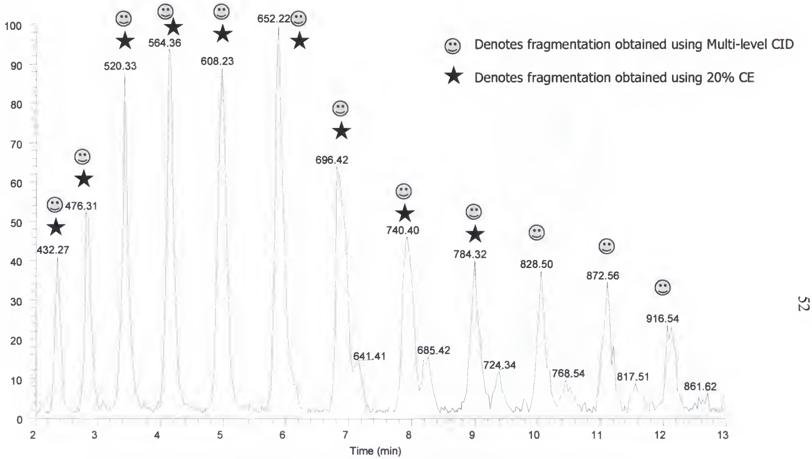

Figure 2-12. An LC/MS/MS analysis of PEG 600 obtained using multi-level CID.

The peaks are labeled to indicate the mass of the PEG and whether good MS/MS data was obtained using either 20% single-level CID or multi-level CID.

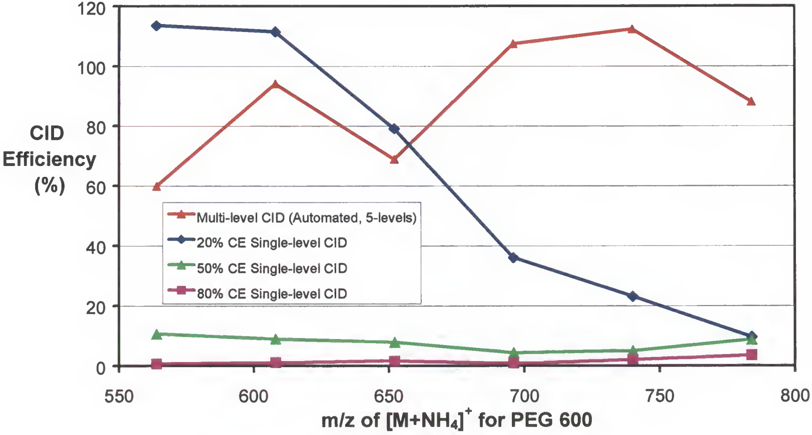

Figure 2-13. CID efficiency for multi-level CID and single-level CID.

The efficiency of CID is plotted for multi-level CID and 3 different collision energies for single-level CID as a function of the mass-to-charge of selected PEG 600 ions. Multi-level CID is the only one with consistently high efficiency.

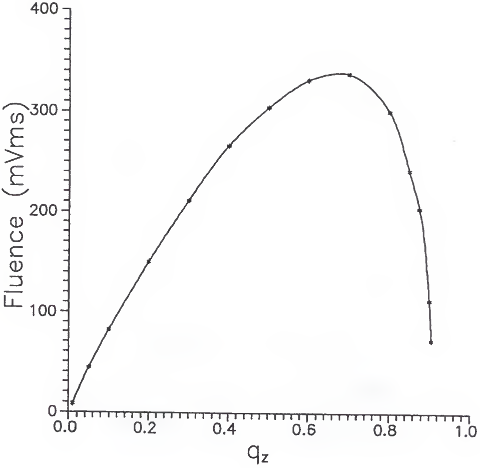

Figure 2-14. A simulation of the depth of the the psuedo-potential well .

This figure is a Hyperion simulation of well depth performed by Randall Pedder. It shows a distinct drop in well depth as the q_z increases above 0.7. (Pedder, 1992)

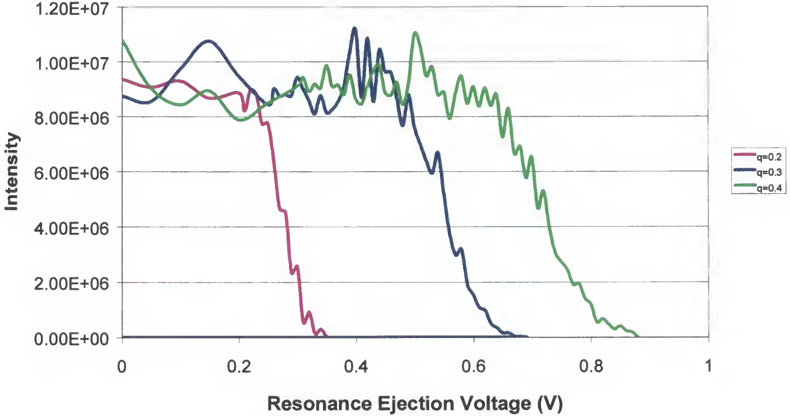

Figure 2-15. Survivor ion curves for the $[M+H]^+$ of benzimidizole.

Survivor ion curves for the $[M+H]^+$ of benzimidizole at q_{ex}=0.2, 0.3,and 0.4 are shown. Though the intensity data are noisy, the voltage where 50% of the initial ion intensity remains easy to discern.

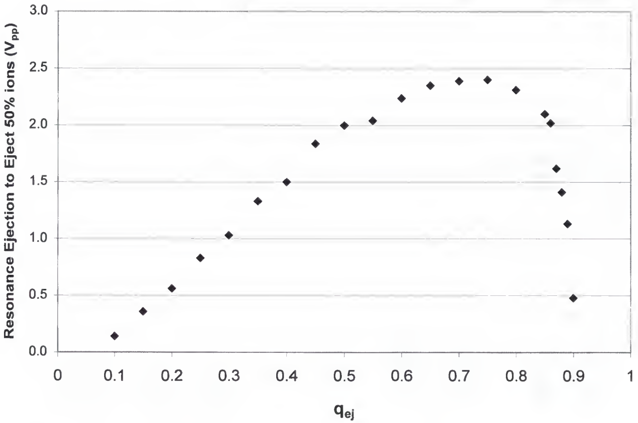

Figure 2-16. The well-depth curve for the $[M+H]^+$ ion of benzimidazole by resonance ejection.

These data were obtained by survivor ion scans at each q_{ej}. The data shows a very similar trend to that predicted by simulation.

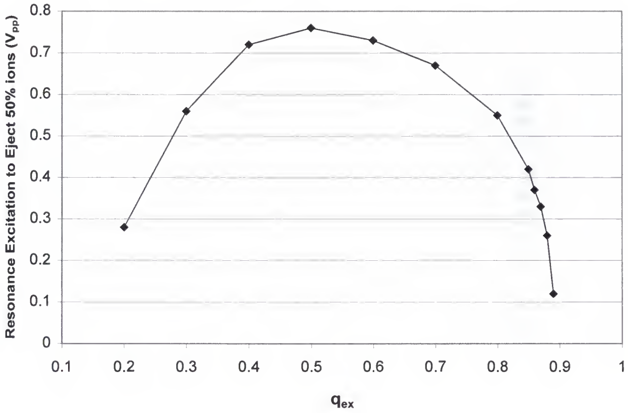

Figure 2-17. The well-depth curve for the $[M+H]^+$ ion of benzimidazole by resonance excitation.

These data were obtained by survivor ion scans which consisted of resonantly exciting the ions at each q_{ex} for 30 ms. The maximum is at a much lower q than that predicted by simulation due to a reduction of intensity by fragmentation of the precursor ion.

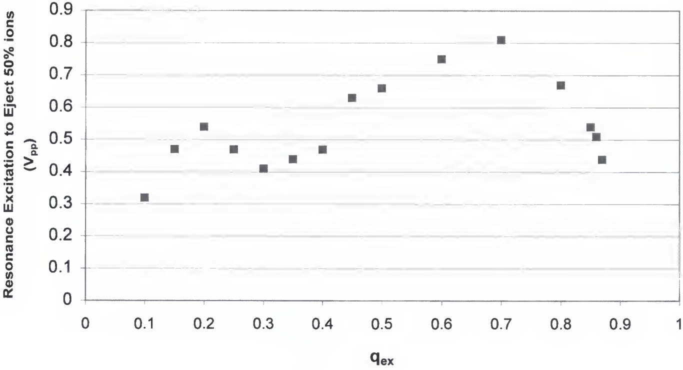

Figure 2-18. The well-depth curve for iodide (m/z 127).

The well-depth curve for iodide shows an unusual dip around q_{ex}=0.3. A similar trend is observed for bromide (m/z 79), but the dip occurred closer to q_{ex}=0.35.

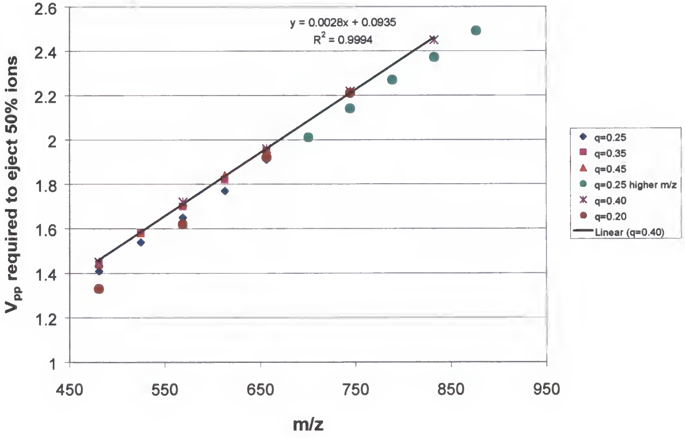

Figure 2-19. A plot of the voltage necessary to eject 50% of the $[M+Na]^+$ ions of PEGs.

Various masses are shown at several q_{ex} values which would be typical for MS/MS. The data are very linear as a function of mass.

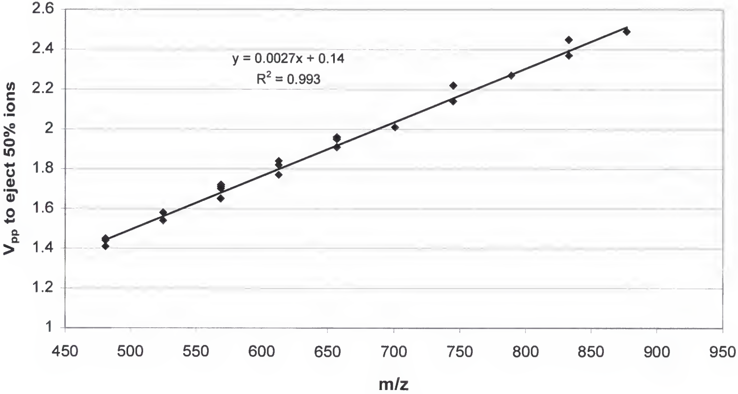

Figure 2-20. A linear fit of voltage to the sodiated PEGs data.

The data from the sodiated PEGs over all q_{ex} values except q_{ex}=0.20 were combined and the linear best-fit equation was implemented as the maximum voltage for multi-level CID.

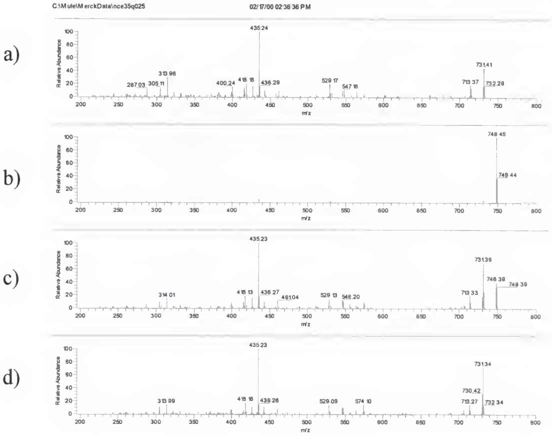

Figure 2-21. A comparison of CID techniques on a tryptic peptide of myoglobin (m/z 749.4)

A tryptic peptide of myoglobin (m/z 749.4) was analyzed by MS/MS using 35% fixed collision energy (a), 30% and 35% normalized collision energy (b and c, respectively), and multi-level CID.

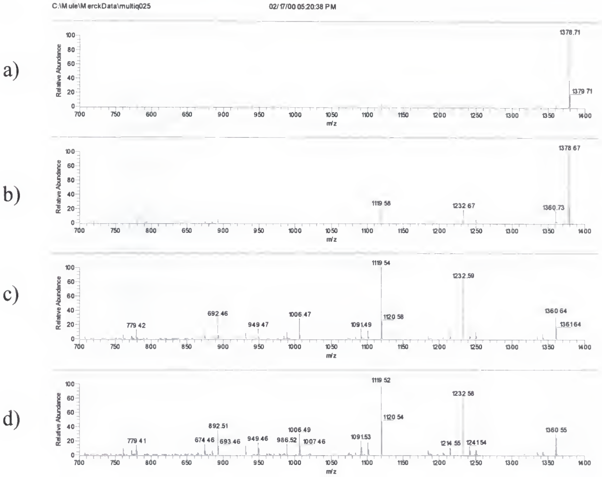

Figure 2-22. A comparison of CID techniques on a tryptic peptide of myoglobin (m/z 1378.7)

A tryptic peptide of myoglobin (m/z 1378.7) was analyzed by MS/MS using 35% fixed collision energy (a), 30% and 35% normalized collision energy (b and c, respectively), and multi-level CID.

CHAPTER 3
HIGH RESOLUTION

This chapter discusses investigations that were undertaken in an attempt to develop exact mass measurement on the quadrupole ion trap. Despite falling short of achieving the goal of exact mass measurement, great strides in improving resolution were made which may contribute to achieving this end in the future.

Overview of High Resolution on the Ion Trap

Mass resolution is a measure of a mass spectrometer's ability to distinguish one mass-to-charge from another. For the commercial quadrupole ion trap, which relies on ion ejection as a detection technique, this means that ions of one m/z need to be ejected before ions of the next m/z. Two main factors will influence the resolution: the spread of ejection times of the ions of the same m/z, and the time between them and the next m/z. The tighter the packet of ions of the same m/z is when it reaches the detector, the better the resolution is. Also, the larger the gap between the packet of ions of consecutive m/z, the better the resolution will be.

Classically, increasing the gap between ion ejection has been achieved by reducing the rate at which the amplitude of the main r.f. is scanned (Kaiser et al., 1989 & Schwartz et al., 1991). Slow scan rates put more time between ions of consecutive m/z reaching the detector.

The bundling of ions of the same m/z into a tight packet is accomplished using resonance ejection (Tucker, 1988). In resonance ejection, a dipolar field is created by a placing a supplemental AC on the endcap electrodes. Ions that share the same m/z also share the same frequency of motion in the ion trap, but they are randomly distributed and moving in different directions. At any point in time, some of the ions of the same m/z may be heading toward the entrance endcap, while others are heading toward the exit endcap. This is not beneficial to resolution since ejection will cause the ions closest to the exit endcap to eject first, leaving the ions which were nearer the entrance endcap to traverse the length of the trap before they can be detected.

Fortunately, resonance ejection helps to overcome this problem. Ions whose frequency of motion in the axial direction matches the frequency of the resonance ejection field begin to move together to form a bundle of ions. This is accomplished because of the dipolar nature of the resonance ejection field. Since the endcaps are 180° out of phase with each other, one endcap is positive while the other is negative. All of the positive ions whose frequency match that of the resonance ejection frequency move away from the positive endcap and toward the negative one (opposites attract). Even though these ions may have started out heading in opposite directions, they are now compelled to move in the same direction at the same time due to electrostatics. The more periods of the resonance ejection frequency that the ions experience, the tighter the ion packet gets and the better the resolution becomes (Schwartz et al., 1991).

Two things that help to define the number of periods that ions of a given m/z will experience are the scan rate of the main r.f. and the amplitude of the resonance ejection frequency (the strength of the dipolar field) (Schwartz et al., 1991). The scan rate of the main r.f. dictates how many periods of the resonance ejection frequency that ions will experience because it is the driving force behind the q of the ions. Since the q of the ions ultimately determines the frequency of the ions, slowly changing an ion's q_z keeps it near the same frequency for a longer period of time. This allows those ions which are similar in frequency to the resonance ejection field to absorb energy from it and begin to move in unison. How the amplitude of resonance ejection affects the number of periods an ion experiences is less obvious.

Imagine a surfer out in the ocean trying to catch a wave that will bring him back to the beach. If the waves come along at regular intervals, they are analogous to the resonance ejection frequency. A series of small amplitude waves will eventually allow the surfer to reach the beach, but one big wave will get the surfer to the beach in short order. Similarly, a series of small amplitude waves will allow ions to increase their distance from the center of the trap and eventually be ejected. A large amplitude resonance ejection field will give the same ions enough energy to be ejected immediately. However, it does not allow time for forming a tight packet of ions all moving in the same direction. For this reason, a small resonance ejection amplitude is better for resolution (Schwartz et al., 1991).

Another factor which impacts resolution in an ion trap is known as "space charge." Space charge is the ion-ion interaction that occurs when too many ions are put into the ion trap (March & Hughes, 1989). Putting too many similarly charged ions into a confined space (such as an ion trap) causes those ions to repel each other. These repulsions cause the motion of the ions to be perturbed and once the motion is perturbed, the frequency of that motion changes. Once the frequency of motion of the ion changes, its assigned mass will also change due to the way that ejection is performed. Space charge causes broad peaks with mistaken mass assignment. It is one of the most critical factors that limits the performance of the quadrupole ion trap.

A good analogy for space charge in the ion trap is considering the ion trap as a bucket. When the bucket is half-filled with water, it is easy to carry the water and pour it out without any spilling. However, space charge is equivalent to filling the bucket to the brim. It degrades the performance of the bucket (Cole, 1997).

With the above information in mind, it seemed to be an easy task to obtain high resolution on an ion trap. The "Slow, Low, No" method of obtaining high resolution required only a slow scan rate, a low resonance ejection amplitude, and no space charge. Unfortunately, there are difficulties that arise when trying to do high resolution.

Difficulties with High Resolution

Most of the difficulties encountered when attempting to do high resolution arise from the reduced scan rate.

The main r.f. amplitude for the LCQ is controlled by a 16-bit digital-to-analog converter (DAC). This DAC has 65,536 discrete steps that generate a 0-10V signal which is later amplified to produce the r.f. voltage which is put on the ring electrode. Scanning quickly over these discrete steps gives a linear sweep on the amplitude of the main r.f. Scanning slowly may cause the voltage on the ring electrode to jump from one voltage to another because the DAC is spending too much time on each individual step. This phenomenon is known as "stepping" the DAC.

Stepping the DAC is somewhat analogous to a broken escalator. If the escalator is functioning properly, an observer would see the people on the escalator being swept smoothly from the bottom floor to the top floor. The escalator's discrete steps are moving quickly enough to provide a smooth ride. If, however, the escalator was stopped or slowed, people would walk up the steps and there would no longer be a smooth flow between the floors.

Another difficulty caused by a slow scan rate is diminished signal intensity because the ion current generated at the detector gets spread out in time. For a constant number of ions reaching the detector, a fast scan rate will have a more intense signal because the ions arrive in a short amount of time. Slow scan rates spread that signal out and, correspondingly, reduce the maximum intensity.

Lastly, ions become more susceptible to space charge effects when employing a slow scan rate (March & Todd, 1995). The low mass-to-charge ions have to push through the ion cloud of higher m/z ions during ejection. During a fast scan, there is not much time for the ions to interact and perturb each other's motion. During a slow scan, however, there is adequate time so the number of ions in the trap has to be reduced to avoid this problem.

Of course, this reduction of ions further weakens an already reduced signal intensity. It therefore becomes necessary to perform substantial averaging of spectra so that the signal emerges from the background noise.

Early High Resolution Work with the LCQ

The LCQ was an excellent platform to conduct high resolution studies. Currently, the Finnigan MAT LCQ has the built-in capability of performing high-resolution (~0.3 Da at FWHM) for charge-state identification (up to ±4) of electrosprayed ions using the "Zoomscan" function. The LCQ provides a number of critical features which were absent in previous ion trap systems. Specifically, these features include:

- Stable r.f. electronics
- Software control of the r.f. scan rate
- Software control of the data acquisition rate, independent of r.f. scan rate
- Software control of supplemental AC frequency and amplitude, including optimization as a function of m/z and r.f. scan rate
- Waveform isolation

Early investigations were simply extending the Zoomscan feature (normally 3.6 ms/Da) to slower scan rates to see how well the LCQ could perform.

Even initial results revealed a problem with simply reducing the scanrate. Figure 3-1 is a plot of the peak width of the $[M+H]^+$ of caffeine (m/z 195) as a function of scan rate. It is clear that an initial reduction of the scan rate (higher ms/Da) gives a narrower peak width, which corresponds to better resolution. However, as the scan rate is slowed even further, this reduction in peak width levels off and there are no further gains with slower scan rates.

A possible explanation for this behavior is that the data were acquired with a fixed resonance ejection amplitude. The resonance ejection amplitude not only needs to be increased as a function of increasing m/z, but also needs to be reduced for slower scan rates. Figure 3-2 shows the behavior of peak width as a function of resonance ejection amplitude at several scan rates for the $[M+H]^+$ of 4-(*p*-nitrobenzyl)pyridine. The optimum resonance ejection amplitude for any given scan rate is the point at which the lowest peak width is obtained. Note that at slower scan rates (higher ms/Da) it becomes more difficult to determine the voltage for the smallest peak width; nevertheless, slower scan rates optimize at lower resonance ejection voltages.

Armed with the optimum resonance ejection amplitude for 4-(*p*-nitrobenzyl)pyridine at various scan rates, a new study of peak width as a function of scan rate was undertaken. Again, the peak width was initially reduced, only to level off at slower scan rates as can be seen in Figure 3-3.

An alternate explanation of space charge was considered to be the culprit in this case. Therefore, the space charge phenomenon needed to be studied. Using three different concentrations, the peak width of the $[M+H]^+$ of caffeine was studied as a function of ion injection time. The more time that ions are allowed into the trap, the more space charge should be a problem; with concentrations of 0.02, 0.05, 0.11 mg/mL of caffeine, there should be more ions getting trapped at any given ion injection time with the higher concentrations.

An unexpected result came from this study, however. The peak widths of the caffeine actually diminished with more ions being trapped. Figure 3-4 shows that the peak widths at 50% of peak height diminished not only as a function of increased ion time, but also as a function of increased concentration. This was the exact opposite of what was expected.

Some simple checks were done on the data to make sure that there was not some sort of instrumental problem. The linearity of the response for each solution was plotted as a check to make sure the detector was not saturated (see Figure 3-5). There were no apparent problems with linearity so the data appeared valid.

Conversations with Mike Senko of Finnigan MAT revealed that the ion trap experiences a phenomenon which is generally identified with ion cyclotron resonance (ICR) mass spectrometers. That phenomenon is known as peak coalescence (Naito &

Inoue, 1996). When ions of the same or slightly different mass-to-charge ratio are trapped together, their frequencies of motion are so close that they merge together and oscillate at a frequecy which is a weighted average of their masses (Jungmann et al., 1987). The ions come together to form a tight packet, but the obtained peak widths are not really representative of resolution since the ions are indistinguishable. This phenomenon may explain the unusual result which was obtained from the ion time study. In fact, closer inspection of the data seems to suggest that the widths of the peaks near the baseline do increase with ion time as expected, but the FWHM decreases.

Resolving Power vs. Resolution

With the newly discovered possibility that ions of similar mass to charge would only coalesce, it became necessary to discover what the resolving power of the ion trap is. Resolving power and resolution are terms which are often used interchangeably, but there is a distinct difference. Resolution can be calculated with only one peak. It requires only a peak width. Resolving power is the ability of a mass spectrometer to actually separate ions of different mass-to-charge. The resolution is a theoretical indication of resolving power, but as seen with the peak width of caffeine, it can be misleading. Upon investigation some sources feared that the resolving power of the quadrupole ion trap was much lower than the literature values of quoted resolution would indicate.

In order to determine if two isobaric ions (ions with the same integer mass) could be separated in the ion trap, an experiment with caffeine and glucuronic acid was performed. Caffeine ($C_8H_{10}N_4O_2$, exact monoisotopic mass=194.0804) and glucuronic acid ($C_6H_{10}O_7$, exact monoisotopic mass=194.0426) are only 0.0378 Da (37.8 mDa) apart. A solution which contained both of these dissolved in 1:1 methanol:water with

0.1% formic acid was infused into the LCQ. The scan rate and resonance ejection amplitude were painstakingly varied until some separation was obtained. Figure 3-6 shows the uncalibrated mass spectrum of these two compounds that was obtained with a scan rate of 400 ms/Da and 0.55 V resonance ejection. It is interesting to note that the first peak is much wider than the second peak. This is keeping with the concept of space charge. Ions of lower m/z are affected by those of higher m/z, but the higher m/z ions don't experience space charge because the lower m/z ions have already been ejected.

To help confirm the identity of this pair of peaks, additional caffeine was added to the mixture to increase its peak height. Since the caffeine is the heavier mass, the second peak displayed a noticeable increase in intensity, as shown in Figure 3-7. At this point, the resolving power of the quadrupole ion trap no longer seemed to be a potential concern.

An interesting point about the data in Figure 3-7 is that there are additional peaks that follow the tall caffeine peak. These peaks, which are approximately 35 mDa apart, are too close in mass to caffeine to be isotopes of either glucuronic acid or caffeine itself. The presence of these suspicious peaks encouraged a closer examination of the data. It was discovered that at 400 ms/Da, the main r.f. DAC was almost certainly "stepping" as opposed to sweeping. Figure 3-8 is an overlay of the where the DAC steps would be with the caffeine spectrum from Figure 3-7. Each of the suspicious peaks falls nicely on a individual DAC step, which occurs every 34.8 mDa. In all likelihood, all of the peaks are actually a single peak that is being artificially segmented because of the stepping DAC. The data from the glucuronic acid and caffeine experiment are not really showing ions of 37.8 mDa being resolved.

Frequency Sweeps

With the disappointing results obtained from a traditional mass-selective instability scan, an alternative way of ejecting ions from the ion trap that did not rely on a DAC was investigated briefly. A frequency sweep involves leaving the amplitude of the main r.f. fixed while the frequency of the resonance ejection is changed.

There is one main difficulty associated with performing frequency sweeps. Specifically, it is an inherently non-linear process since the secular frequency of the ions is dependent on β which is dependent on the square of q. For ions to eject in an increasing m/z fashion as in a normal mass spectrum, the frequency of resonance ejection needs to be swept from a high frequency to a low frequency since q and β are inversely related to m/z. As the frequency gets lower, the spacing in frequency of different masses also get smaller. Thus, good resolution may be obtained at high q values, but as the frequency approaches low q values, it will degrade quickly. This means that frequency sweeps are only useful over a small mass-to-charge range.

The most successful way of implementing frequency sweeps was to identify a particular mass-to-charge of interest as a center mass, set that mass at a particular q, and assign a scan window around it. Figure 3-9 gives an example of a typical spectrum of caffeine using frequency sweeping. The caffeine's $[M+H]^+$ was placed at a $q_z=0.83$ and the q of the first mass and last mass of the scan was calculated from $m_1q_1=m_2q_2$. Armed with the q of the first and last mass, it is an easy task to calculate the necessary frequencies to sweep in order to produce a mass spectrum.

Overall, the frequency sweep did not appear to be any better than mass-selective instability so it was soon abandoned.

Final Results of High Resolution on the LCQ

In order to get around the problem of stepping the main r.f. DAC, two approaches were undertaken somewhat simultaneously.

Vernier DAC

The main r.f. circuit of the LCQ is equipped with two identical 16-bit DACs. The resistance following the second DAC, which is unused in any current LCQ applications, is 15.8 times greater than the resistance that follows the main r.f. DAC. This allows the second DAC to generate voltages from zero to 0.63 V, instead of 0–10 V, with its 65,536 steps. The main r.f. circuit sums the voltages from both DACs before it is amplified and sent to the ring electrode. Thus, the second DAC is a vernier DAC: it is capable of taking much finer steps than the main DAC.

By implementing the vernier DAC, it would be possible to use scan rates which were previously causing stepping. The hope was that the leveling off of peak width as a function of scan rate would now continue to show smaller peak widths.

To test the software implementation of the vernier DAC, spectra of caffeine were obtained at 400 ms/Da using just the main DAC and then the vernier DAC at several different ion injection times. Figure 3-10a shows a badly segmented peak for the $[M+H]^+$ of caffeine when using only the main r.f. DAC. However, a dramatic improvement can be seen in Figure 3-10b. Even though the monoisotopic peak is misshapen when the Vernier DAC is implemented, the ^{13}C isotope shows good peak shape. The misshapen monoisotopic peak was a result of space charge; at lower ion times, both the ^{12}C and ^{13}C peak demonstrated good peak shape.

With the successful implementation of the vernier DAC, another study of peak width as a function of scan rate was undertaken. This time, there would be no worry of

DAC stepping. An additional parameter was also controlled during this experiment. As the scan rate is slowed, the bandwidth of the electrometer (detector) circuit needs to be lowered to filter out noise. Reducing the bandwidth too much leads to oversmoothing and could actually broaden the width of the detected peaks. For this experiment, the scan rate was slowed 50% for each step while the bandwidth of the electrometer was reduced by 20%. In addition, the automatic gain control (AGC) function was activated to provide a constant number of ions into the ion trap.

Figure 3-11 shows the results of decreasing the scan rate with the vernier DAC. Comparing Figure 3-11 to Figure 3-1, it is clear that the peak width continued to drop at scan rates where it had previously leveled off. However, there was still a point of diminshing returns even with the vernier DAC implemented.

Fortunately, more positive results were gained from the second approach to avoid DAC stepping.

Development of A Novel Ion Ejection Technique

Each of the two previously used ejection techniques has drawbacks. Mass-selective instability with resonance ejection relies upon a DAC to increase the amplitude of the main r.f. on the ring electrode so that ions will be pushed toward an artificial ejection boundary defined by the resonance ejection frequency. The resolution is essentially constant across the entire mass range, but the DAC limits the slowest scan rate possible. Frequency sweeps use a dynamically changing ejection boundary and do not suffer from the constraints of a DAC, but the frequencies of high masses begin to compress at lower q's causing a loss of resolution and a non-linear mass scan. Since there are difficulties associated with the two traditional ways of ejecting ion from an ion trap, a novel ion ejection method was developed.

A combination of the two traditional ejection techniques, known as HI-RES, was developed that would alleviate some of the difficulties experienced with each one individually.

HI-RES (Highly Improved Resonance Ejection Scan) is a novel technique which uses two conventional ion ejection strategies in conjunction to give unsurpassed resolving power. By combining mass selective instability with a dynamically changing resonance ejection frequency, the timing of ion ejection is altered and resolution is improved.

HI-RES works on the principle of relative rates. The main r.f. amplitude is being scanned at a fixed rate. The resonance ejection frequency is also being scanned at a fixed rate in the same direction as the main r.f. If the rates of these two scans are slightly different, then the rate of ion ejection that is achieved would be slower than either of the two ejection techniques could achieve individually.

As an example, lets consider two cars moving along a highway at 65 and 70 mph. From a static frame of reference, both cars may be moving very fast. From the point of view of the first car, doing 65 mph, the second car is passing only slowly. The absolute rates of both cars are high, but the relative rate of one car to the other is very slow.

Figure 3-12 is an illustration of HI-RES. The ions are marching toward higher q due to the increasing r.f. amplitude on the ring electrode while the resonance ejection frequency is also moving toward higher q. In this illustration, the resonance ejection frequency is moving slightly more slowly than the ions, so the ions will be ejected in the correct m/z order. Of course, there are other ways to implement this type of scan too.

There are four ways of implementing the HI-RES ejection technique. Both the main r.f. and the resonance ejection frequency can be moving toward higher or toward lower q (two possibilities). In either case, either the r.f. or the resonance ejection frequency must be moving faster than the other one (two choices for each of the earlier possibilities).

Figure 3-13 is a plot which was developed to help aid the understanding of what HI-RES is doing. The secular frequencies of relevant ions in the scan have been calculated from their q values and the frequency of each ion has been plotted as a function of time. The spectrum obtained for the scan has been overlaid with the frequency of each ion as well as the frequency of the resonance ejection signal. When the secular frequency of an ion crosses the frequency of resonance ejection, it is ejected and detected, as can be seen in the spectrum.

Figure 3-14 shows a comparable plot using the Zoomscan function. Zoomscan is a classic mass-selective instability scan at a reduced scan rate. The resonance ejection point for Zoomscan is fixed at q_z=0.83, which corresponds to a frequency of 279.8 kHz. The timing between the ejection of the isotopes is much shorter for mass-selective instability than it is for HI-RES, even though the r.f. scan rates are identical.

Combining mass-selective instability and frequency sweeping has led to unprecedented resolving power on the quadrupole ion trap mass spectrometer. Figure 3-15 shows a comparison between a Zoomscan and a HI-RES scan of the $[M+5H]^{+5}$ of bovine insulin. The main r.f. was scanning at the same rate (dV/dt) in both spectra, but the HI-RES had the added benefit of a dynamically changing resonance ejection frequency.

HI-RES was tested on numerous compounds and charge states to see how good the resolving power really is. Figure 3-16 to 3-20 are typical examples of spectra achieved using HI-RES. Each mass spectrum has been calibrated off-line so that an overlay with the theoretical isotopic distribution obtained from IsoPro v3.0 (Senko, 1997) could be included. The conditions for each spectrum are included in the figure caption.

The scan rate for each spectrum is listed in ms/Da, though strictly speaking this is incorrect for the HI-RES scan. The LCQ requires a scan rate is ms/Da and the rate provided is the rate entered into the LCQ. Since the timing of ejection is changed by moving the resonance ejection frequency in conjunction with the main r.f. amplitude, the actual scan rate varies across the length of the scan and is dependent on factors such as scan width, scan rate, and the range of frequencies that the resonance ejection signal sweeps.

Comparison of HI-RES to Mass-selective Instability

With the improved results obtained using HI-RES, it is only natural to perform a comparison to traditional mass-selective instability with resonance ejection. In order to perform such a comparison, the analyte ions must be selected such that mass-selective instability is capable of resolving the isotopic peaks, at least partially. Therefore, the +5 charge state of bovine insulin was used to compare these two ejection techniques in the area of space charge, scan rate, and trap pressure.

The effect of space charge was monitored by recording the peak width of five of the $[M+5H]^+$ isotopes over several ion injection times. The peak width at 80% maximum peak height was measured since mass-selective instability would not be able to separate the isotopes at 50% peak height. The average of the 5 peak widths was plotted with error bars of ± one standard deviation. The results of this study are present in Figure 3-21. It should be noted that the peak width at the maximum ion time (2 ms) could not be measured due to inadequate separation of the isotopes.

While it is tempting to state that space charge is better tolerated using HI-RES, this study is by no means conclusive. In fact, both curves tend to increase at about the same rate indicating that both ejection techniques suffer equally from space charge effects. It is fair to say, however, that for a given ion injection time, HI-RES can provide better resolution.

With regard to scan rate, the familiar behavior of an exponential decay is evident in Figure 3-22 for both ejection techniques. This scan rate study was perhaps the best study of this type conducted since all of the pertinent parameters were being appropriately controlled. Not only was the resonance ejection amplitude optimized for each scan rate, but the bandwidth and the sampling rate of the electrometer were set to the correct theoretical values for the LCQ using the equations below:

$$BAND(Hz) = \frac{1}{scanrate(s/Da)}$$

$$SAMP(pts./Da) = 100{,}000 \times scanrate(s/Da)$$

The 100,000 is the maximum rate (in Hz) that the analog-to-digital converter of the acquisition board can convert data. Previous studies controlled these parameters, but not quite at their optimum settings.

Finally, the effects of bath gas pressure in the trap were studied on both ejection techniques. The helium pressure in the ion trap of the LCQ is controlled by a regulator which applies 5 psi of head pressure to a 24 inch piece of fused silica (100 μm i.d.). For this experiment, the head pressure on this restrictor was set to 2, 7, 9, 11, 13, and 15 psi. The pressure was read from a gauge that had been previously installed after the built-in

LCQ regulator. By calculating the flow of helium through the capillary restrictor (Thompson, 1994), the trap pressure can be obtained.

In order to calculate flow, the viscosity of the helium must first be obtained from

$$\eta = (4.05 \times 10^{-7})T + 7.58 \times 10^{-5} \tag{3-1}$$

where

η=helium viscosity, dyn•s/cm^2

T=temperature, K.

Flow is also dependent on the average linear velocity, V_{avg}, through the capillary restrictor into vacuum (Thompson, 1994).

$$V_{avg} = \frac{3(r/2)^2(P + 14.7) \times 68947}{32L\eta} \tag{3-2}$$

where

V_{avg}=average linear velocity, cm/s

r=capillary i.d., cm

P=capillary inlet pressure, psi (atmospheric)

L=capillary length, cm.

The flow, F, through the capillary (Guckenberger, 1999) is

$$F = 60r^2 V_{avg}\pi \left[\frac{298}{T}\right]\left[\frac{2(P + 14.7)}{3 \times 14.7}\right] \tag{3-3}$$

The trap pressure is then calculated from

$$P_{trap} = \frac{F}{60 * 1000} \times \frac{760}{C} \tag{3-4}$$

where C is the conductance out of the trap in L/s (Guckenberger, 1999). For the LCQ, the conductance is ~3.74 L/s.

Figure 3-23 shows the results of the pressure study. This is perhaps the most telling figure in the dissertation. There is a dramatic rise in the peak width as the pressure increases for mass-selective instability. HI-RES, however, only has a moderate rise even at extreme pressures. It is important to note that the last point for mass-selective instability has no error bars because there was only one peak which was resolved to 80% peak height.

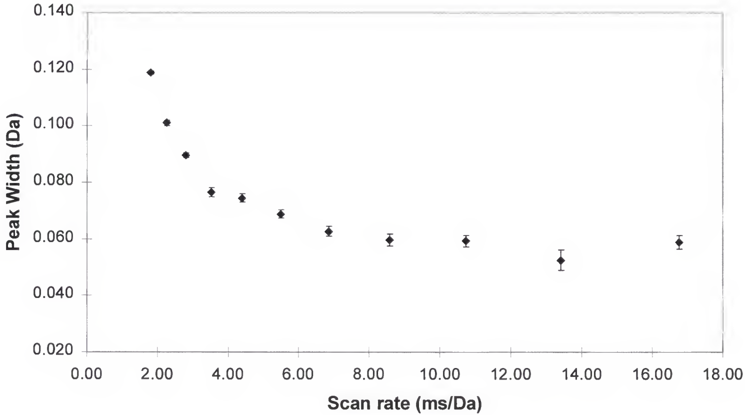

Figure 3-1. Peak width as a function of scan rate for caffeine.

The average peak width (± one standard deviation) of the $[M+H]^+$ ion of caffeine (m/z 195) is shown as a function of scan rate.

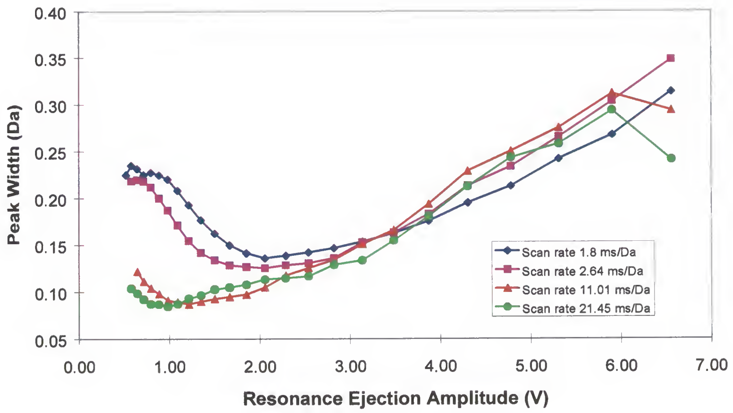

Figure 3-2. Peak width as a function of resonance ejection amplitude.

The peak width for the $[M+H]^+$ ion of 4-(p-nitrobenzyl)-pyridine is shown at four scan rates as a function of the resonance ejection amplitude. The optimum amplitude to use for any scan rate is the point where the peak width dips to it lowest value. Note that at slower scan rates it becomes more difficult to determine the voltage where the dip occurs.

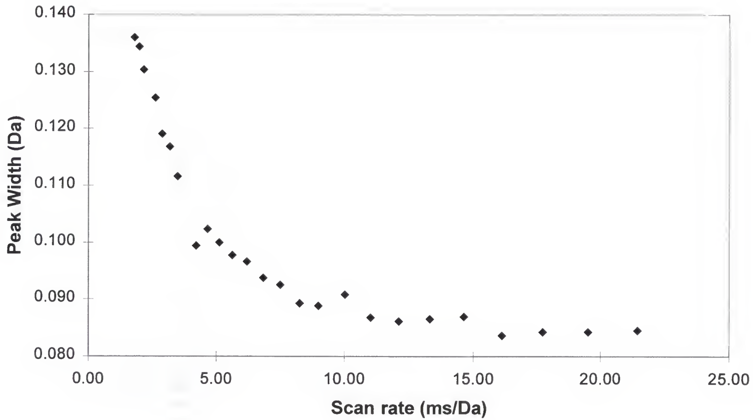

Figure 3-3. Peak width as a function of scan rate for 4-(*p*-nitrobenzyl)-pyridine.

The peak width of the $[M+H]^+$ ion of 4-(*p*-nitrobenzyl)-pyridine (m/z 215) is shown as a function of scan rate. There are no error bars because only the peak width for the optimized resonance ejection amplitude is plotted for each scan rate. Similar to caffeine's peak width behavior, the initial reduction eventually levels off at slower scan rates.

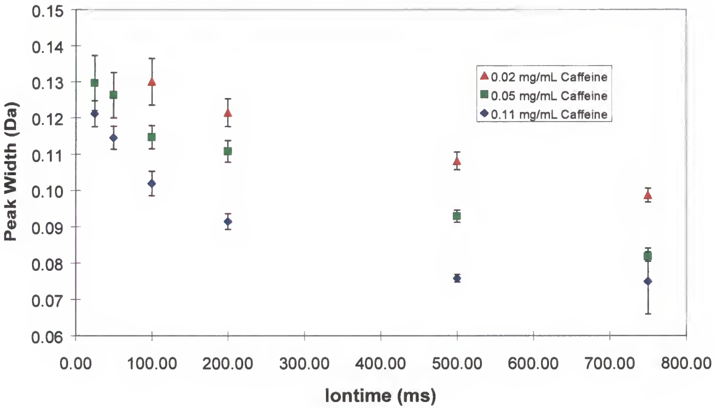

Figure 3-4. Peak width versus ion injection time for caffeine.

The average peak width (±1 standard deviation) for the $[M+H]^+$ of caffeine (m/z 195) is plotted for three different concentrations of caffeine solution as a function of ion injection time. At high ion times and concentrations, more ions are trapped, but the data do not show a corresponding increase in peak width; rather, it shows a decrease.

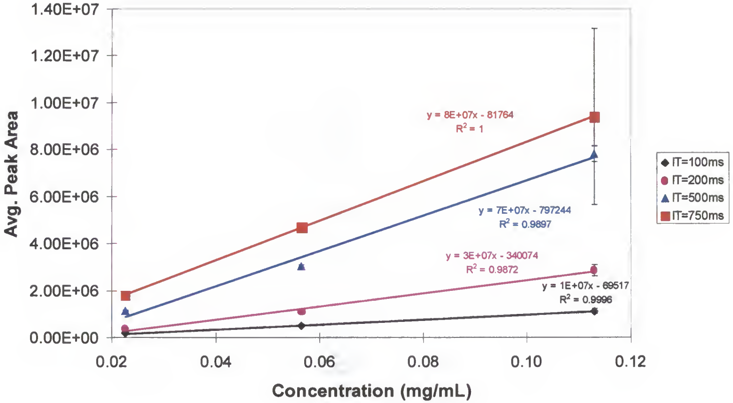

Figure 3-5. Linearity curves for caffeine.

The average peak area (±1 standard deviation) for the $[M+H]^+$ ion of caffeine is plotted for four ion injection times as a function of caffeine solution concentration. The linearity of each curve is good, suggesting that the detector is not saturated. The large deviation in the 750 ms point at 0.113 mg/mL is due to instability in the electrospray source.

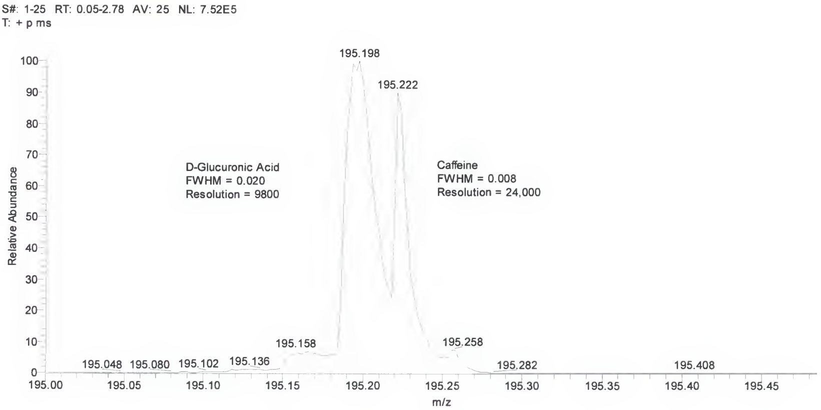

Figure 3-6. Mass spectrum (uncalibrated) of caffeine and glucuronic acid.

Caffeine and glucuronic acid, which differ in mass by 37.8 mmu, were dissolved in 1:1 methanol:water with 0.1% formic acid and infused into the LCQ. The scan rate was 400 ms/Da with a resonance ejection amplitude of 0.55 V.

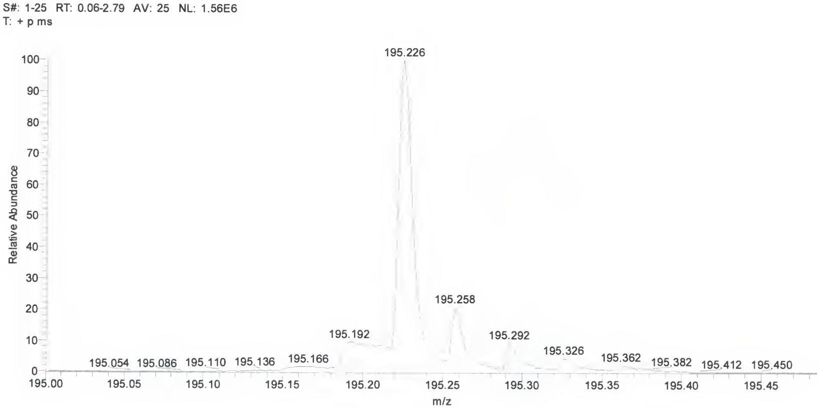

Figure 3-7. Mass spectrum (uncalibrated) of caffeine and glucuronic acid with additional caffeine.

Additional caffeine was added to the solution used in Figure 3-6. The added caffeine would contribute to an increase in the second peak of the doublet from Figure 3-6, as is observed here, since the m/z of caffeine's $[M+H]^+$ is higher than that of glucuronic acid. Note the addition of smaller peaks at higher mass.

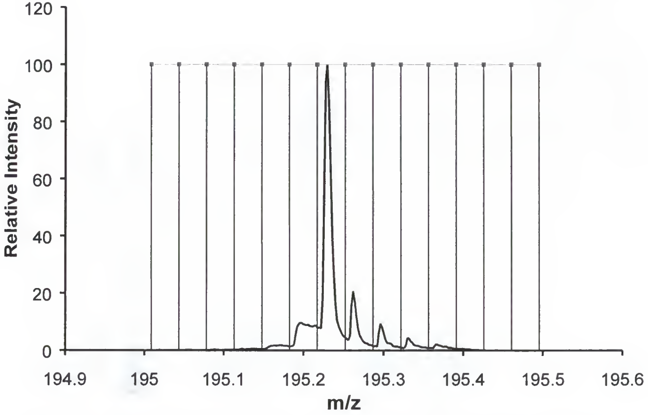

Figure 3-8. Overlay of DAC step size with mass spectrum of caffeine and glucuronic acid.

Figure 3-8 shows the mass spectrum of caffeine and glucuronic acid from Figure 3-7 overlayed with vertical bars that represent the places where the main r.f. DAC would be incrementing. Not surprisingly, there is a pulse of ions during each DAC step indicating that the DAC is being scanned too slowly.

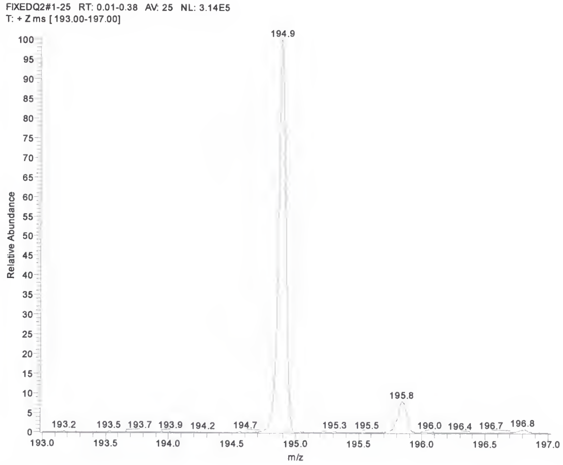

Figure 3-9. Mass spectrum of caffeine obtained using a resonance ejection frequency sweep.

The $[M+H]^+$ of caffeine (m/z 195) was brought to q_z=0.83. The q values for m/z 193 and m/z 197 were calculated by Equation 1-7 and converted to frequencies (279.7 and 269.2 kHz, respectively). The resonance ejection frequency was then scanned at a rate of 20 ms/kHz from one frequency to the other to eject the ions.

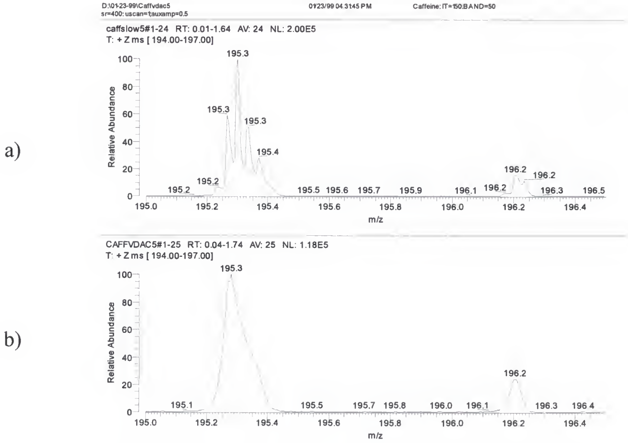

Figure 3-10. Mass spectra of caffeine acquired without (a) and with (b) the vernier DAC.

Both spectra were obtained on the same caffeine solution under the same conditions at 400 ms/Da. In (a), only the main r.f. DAC was scanned to increase the r.f. amplitude . In (b), both the main r.f. and the vernier DAC were used.

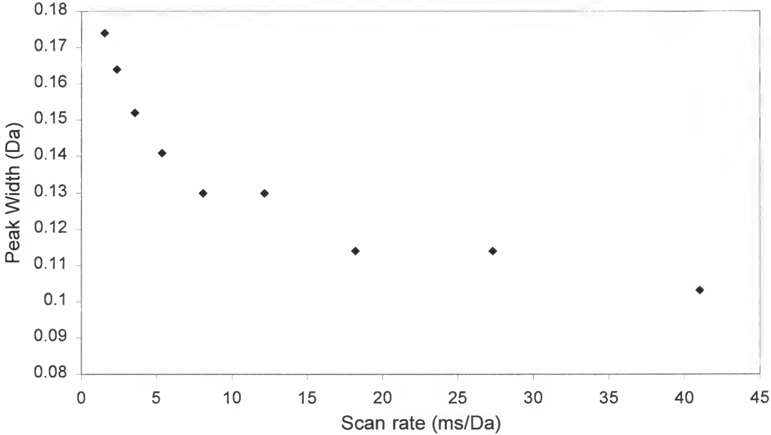

Figure 3-11. Peak width as a function of scan rate for caffeine.

The peak width for the $[M+H]^+$ ion of caffeine was measured manually from a printout of the average of 10 scans at each scan rate. Each scan rate used different values for the resonance ejection amplitude and the bandwidth of the electrometer.

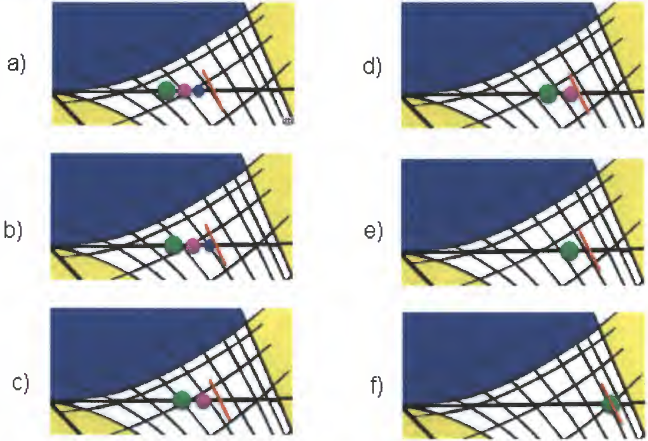

Figure 3-12. An illustration of HI-RES.

Three ions are depicted as spheres along the a_z=0 line of the Mathieu stability diagram. The smaller spheres represent lower mass-to-charge values. The red line represents the artificial stability boundary created by the resonance ejection frequency. All of the ions and the resonance ejection frequency are moving to the right (toward the β_z=1 stability boundary) throughout the series of snapshots (a-f). As an ion catches up to the resonance ejection frequency, it is ejected from the trap.

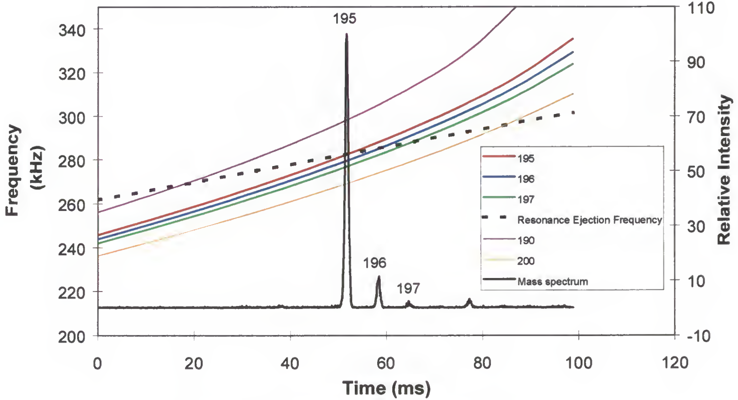

Figure 3-13. Frequency versus time plot for HI-RES.

This plot shows the secular frequencies of selected ions and the resonance ejection frequency as a function of time during a HI-RES scan. It is overlaid with a spectrum of caffeine obtained under these conditions. Note that the peak appears only when the resonance ejection frequency crosses the frequency of the ion. The lines for m/z 190 and m/z 200 represent the beginning and end of the scan.

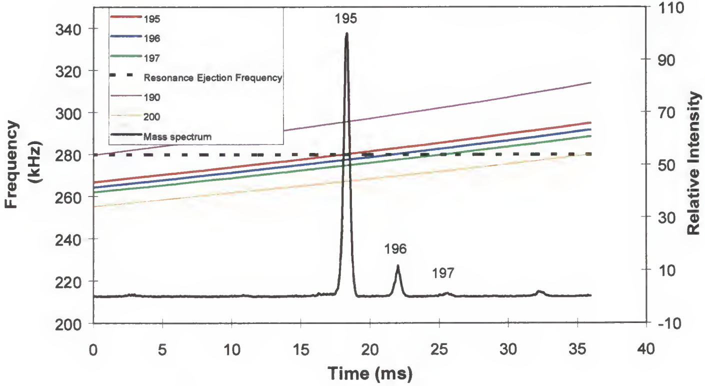

Figure 3-14. Frequency versus time plot for mass-selective instability with resonance ejection.

This figure shows a frequency versus time plot for an LCQ Zoomscan of caffeine. Note the fixed resonance ejection frequency.

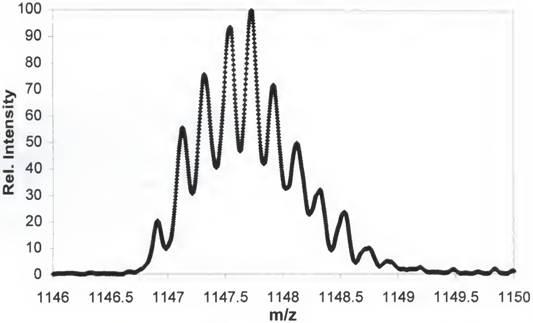

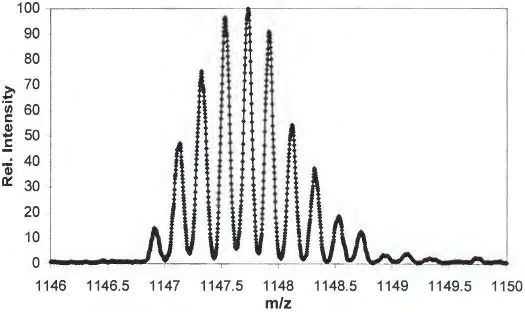

Figure 3-15. Zoomscan and HI-RES spectra of the $[M+5H]^{+5}$ ion of bovine insulin.

The top spectrum shows a typical high resolution experiment (Zoomscan) that is available on the LCQ using fixed resonance ejection at q_z=0.83. The bottom spectrum shows the same ions resolved much better using the HI-RES scan technique where the resonance ejection point was changed from q_z=0.86 to q_z=0.88.

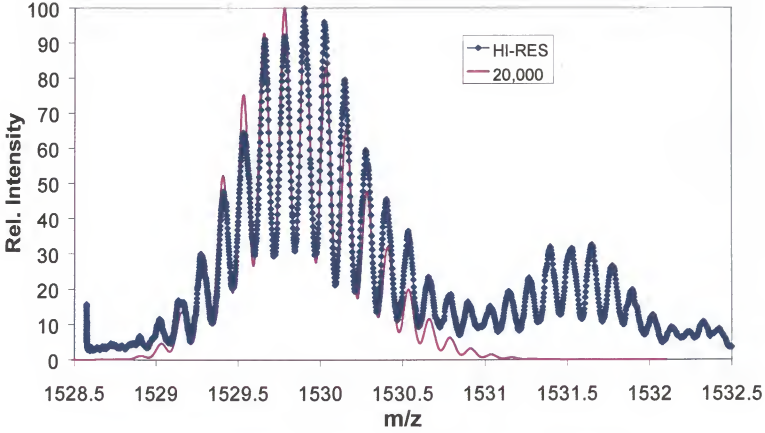

Figure 3-16. HI-RES spectrum of cytochrome c $[M+8H]^{+8}$.

Changing the resonance ejection point from q_z=0.86 to q_z=0.88 at a specified scan rate of 3.6 ms/Da generated a peak width at FWHM of 0.08 Da (19,000 resolving power).

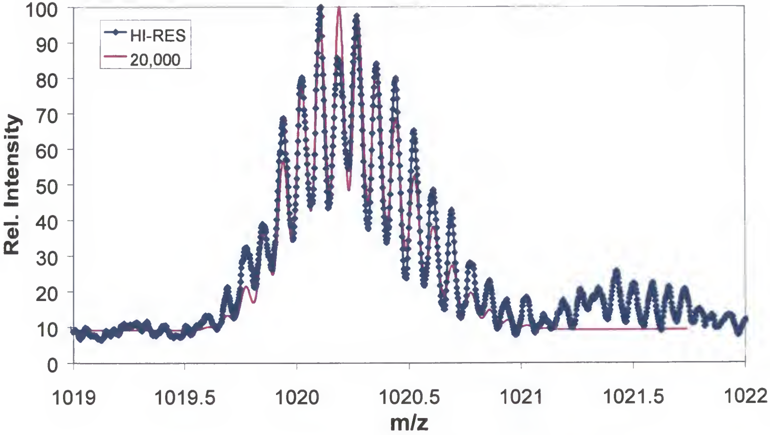

Figure 3-17. HI-RES spectrum of myoglobin $[M+12H]^{+12}$.

Changing the resonance ejection point from $q_z=0.86$ to $q_z=0.88$ at a specified scan rate of 7.2 ms/Da generated a peak width at FWHM of 0.07 Da (15,000 resolving power).

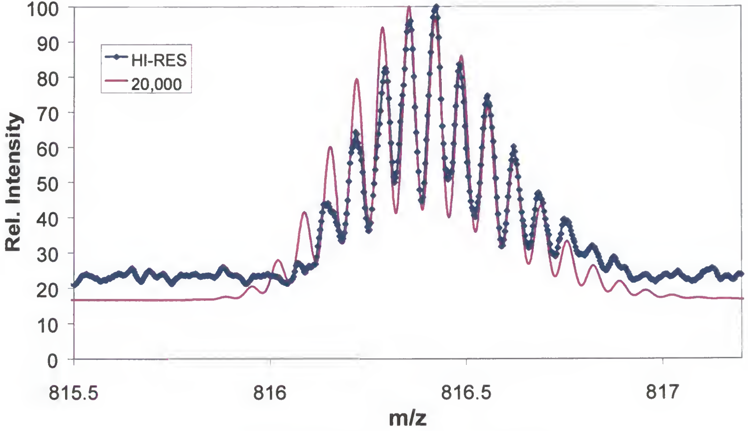

Figure 3-18. HI-RES of cytochrome c $[M+15H]^{+15}$.

Changing the resonance ejection point from q_z=0.80 to q_z=0.86 at a specified scan rate of 14.4 ms/Da generated a peak width at FWHM of 0.04 Da (20,000 resolving power).

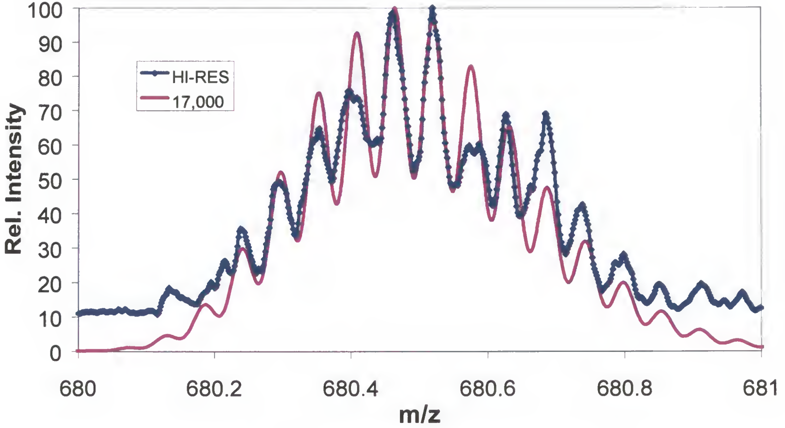

Figure 3-19. HI-RES spectrum of cytochrome c $[M+18]^{+18}$.

Changing the resonance ejection point from q_z=0.86 to q_z=0.88 at a specified scan rate of 28.8 ms/Da generated a peak width at FWHM of 0.04 Da (17,000 resolving power).

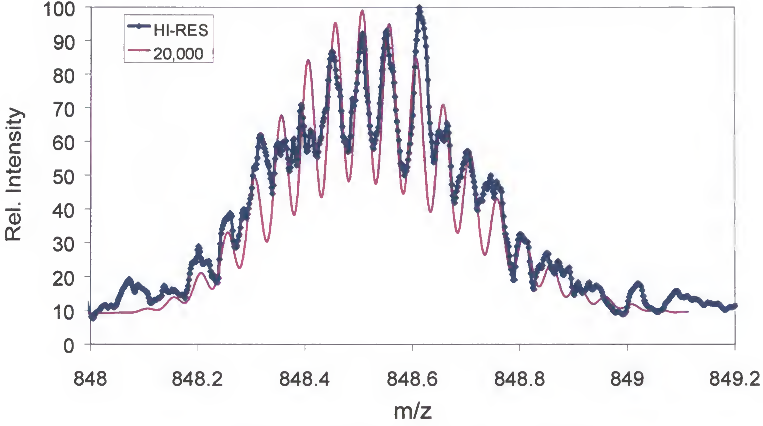

Figure 3-20. HI-RES spectrum of myoglobin $[M+20H]^{+20}$.

Changing the resonance ejection point from q_z=0.86 to q_z=0.88 at a specified scan rate of 36 ms/Da generated a peak width at FWHM of 0.05 Da (17,000 resolving power).

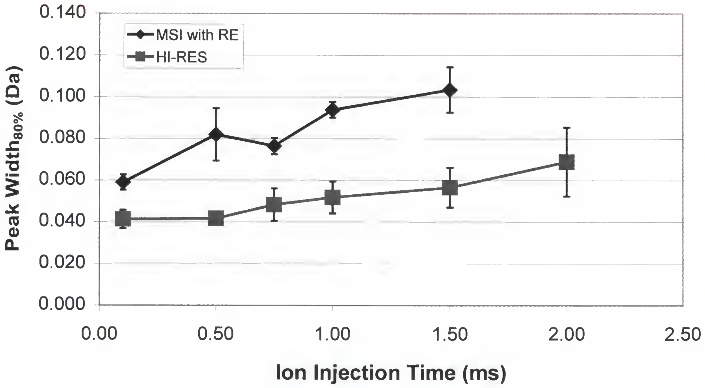

Figure 3-21. The effect of space charge on peak widths.

The average peak width for 5 isotopes of the $[M+5H]^{+5}$ ion of insulin at 80% peak height is shown (±1 standard deviation) for HI-RES and mass-selective instability with resonance ejection as a function of ion injection time. Increasing the number of ions that are injected and trapped increases the effect of space charge causing wider peaks. HI-RES maintains narrower peaks at every injection time.

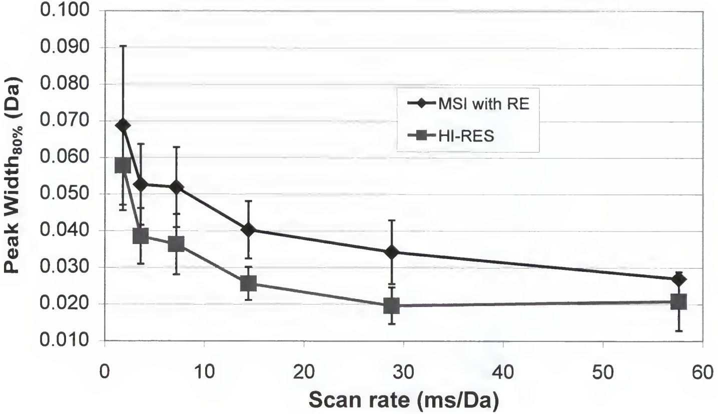

Figure 3-22. Peak widths as a function of scan rate.

The average peak width for 5 isotopes of the $[M+5H]^{+5}$ ion of insulin at 80% peak height is shown (±1 standard deviation) for HI-RES and mass-selective instability with resonance ejection as a function of scan rate. The bandwidth of the electrometer, sampling rate, and resonance ejection amplitude was optimized at each scan rate for both ejection techniques.

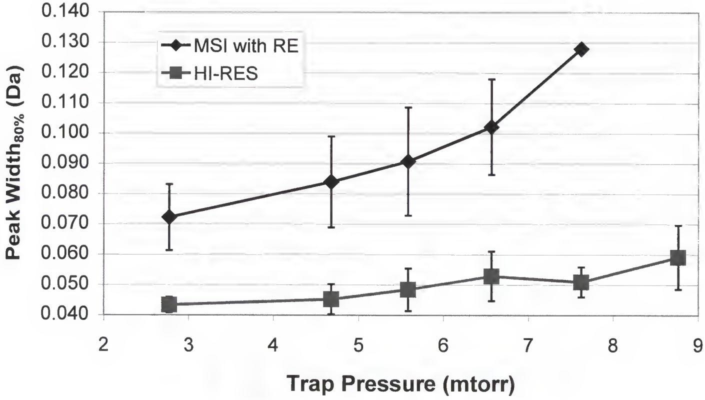

Figure 3-23. Peak width as a function of ion trap bath gas pressure.

The average peak width for 5 isotopes of the $[M+5H]^{+5}$ ion of insulin at 80% peak height is shown (±1 standard deviation) for HI-RES and mass-selective instability with resonance ejection as a function of bath gas pressure. At pressures higher than 7 mtorr, mass-selective instability was unable to resolve more than one isotope. HI-RES, however, is very tolerant of bath gas pressure.

CHAPTER 4
CONCLUSIONS AND FUTURE WORK

Despite the more than fifteen years since the commercialization of the quadrupole ion trap as a mass spectrometer, many facets of its fundamentals are not yet well understood. Its small size and versatility make it an excellent device for mass spectrometry, but its fundamentals are difficult to grasp, leaving room for further study and improvement.

This work has demonstrated a significant enhancement to the abilities of the quadrupole ion trap in two areas: tandem mass spectrometry and high resolution.

Multi-level CID, though an application in nature, is based strongly on the fundamental workings of the ion trap. It relies on three features that are inherent to the ion trap.

First, the use of successively increasing excitation voltages is the only way to minimize ejection of the precursor ion and enhance the possibility of fragmentation. Any other approach risks ejection of the precursor without fragmentation.

Second, the ability to excite only a particular ion, or range of ions, is critical since any product ions that are formed must also be trapped. Though some product ions may be structurally uninformative (i.e. when an ion losses a small neutral molecule such as water), the ion trap is unique in its powerful ability to select a particular product ion and interrogate it as a new precursor ion using MS^n.

Lastly, the psuedo-potential well model of the ion trap proposed by Dehmelt was critical to the successful implementation of multi-level CID. Previous simulations of the nature of the well at high q values were confirmed with experimentation and this information was used to define an appropriate maximum collision energy. Obtaining an appropriate maximum collision energy removed the user and allowed a fully automated approach that could be successfully implemented on a chromatographic time scale.

As time goes on, there will be more efforts made which attempt to improve the efficiency of the CID process.

Recently, Bruker-Franzen has announced a scheme to improve the CID efficiency of their trap that is similar to multi-level CID. It uses an amplitude sweep, rather than several distinct steps. However, the approach is still limited because it is based on a user-supplied collision energy. As the push toward standardizing CID spectra for library searches grows, it will be necessary to have a consistent way of performing CID. Multi-level CID could be that way since it is grounded in the physics of the ion trap.

High resolution for the purpose of performing exact mass measurement on the quadrupole ion trap is yet an unrealized goal. Despite this fact, the development of the HI-RES ejection technique has helped to propel mass spectrometrists closer to that goal.

Investigations into the previous techniques used to achieve high resolution on the quadrupole ion trap revealed diminishing returns as the techniques were pushed to their extremes. Figure 3-23 suggests that the pressure in the ion trap is an extremely critical factor for high resolution. Perhaps it is the limiting factor for the diminishing returns that are obtained when the scan rate is slowed substantially since it is the only parameter that cannot be routinely altered.

Jae Schwartz of Finnigan presented a poster at ASMS where resolution of a +10 charge state was obtained. It was interesting to see that several hardware modifications to the instrument were required in order to achieve . Most of these modifications were designed to reduce the pressure in the trap. For instance, a smaller hole in the heated capillary reduced the base pressure of the instrument and less helium bath gas was allowed to flow directly into the trap.

HI-RES has achieved a +20 charge state without hardware modifications (Figure 3-20). It would be interesting to see what results could be obtained by combining Schwartz's modifications with the HI-RES technique.

Much more work needs to be done on HI-RES, not the least of which is calibration. The HI-RES technique needs to be able to self-generate calibrated data. Currently, all of the data are calibrated off-line; this is only possible when analyzing known compounds.

The calibration of the HI-RES technique will be a difficult task. Even if the same frequencies are scanned for different mass-to-charge ranges, the peak positioning will change because ion of higher m/z are inherently closer in frequency than those of lower m/z. Likewise, fixing the time a HI-RES scan takes would result in better resolution at low m/z because more high m/z ions would be ejected in the same time. A sliding calibration scale, which is sensitive to the range of mass-to-charge values that are scanned, needs to be developed.

Overall, the work conducted has help to expand and enhance the capabilities of the quadrupole ion trap and will hopefully contribute to making the ion trap a more useful tool for the mass spectrometrist.

LIST OF REFERENCES

Creaser, C.S; Stygall, J.W. *Tr. Anal. Chem.* **1998**, *17*, 583-593.

Cole, R.B. *Electrospray Ionization Mass Spectrometry*; John Wiley & Sons: New York, **1997**.

DeGnore, J.P.; Yost, R.A. Presented at the Pittsburgh Conference on Analytical Chemistry and Applied Spectroscopy, Chicago, IL, **1996**; paper 116.

Dehmelt, H. G. *Adv. At. Mol. Phys.* **1967**, *3*, 53.

Dehmelt, H. G. *Rev. Mod. Phys.* **1990**, *62*, 525-530.

Fulford, J.E.; March, R.E. *Int. J. Mass Spectrom. Ion Phys.* **1979**, *30*, 39-55.

Gidden, J.; Wyttenbach, T.; Jackson, A.T.; Scrivens, J.H.; Bowers, M.T. *Proceedings of the 47th ASMS Conference on Mass Spectrometry and Allied Topics* **1999**, 1016-1017.

Guckenberger, G.B. Ph.D. Dissertation, University of Florida, Gainesville, FL, **1999**.

Jungmann, K.; Hoffnagle, J.; DeVoe, R.G.; Brewer, R.G. *Phys. Rev. A* **1987**, *36*, 3451-3454.

Kaiser, R.E.; Cooks, R.G.; Stafford, G.C.; Syka, J.P.; Hemberger, P.H. *Int. J. Mass Spectrom. Ion Processes*. **1991**, *106*, 79-115.

LCQ MS Detector Hardware Manual rev.B; Finnigan MAT: San Jose, **1996**.

Lopez, L.L.; Tiller, P.R.; Senko, M.W.; Schwartz, J.C. *Rapid Commun. Mass Spectrom.* **1999**, 663-668.

Louris, J. N.; Schwartz, J. C.; Stafford, G. C.; Syka, J. E. P.; Taylor, D. M. *Proceedings of the 40th ASMS Conference on Mass Spectrometry and Allied Topics* **1992**, 1003-1004.

Major, F. G.; Dehmelt, H. G. *Phys. Rev.* **1968**, *170*, 91-107.

March, R. E.; Hughes, H. E. *Quadrupole Storage Mass Spectrometry*; John Wiley & Sons: New York, **1989**.

March, R. E.; Todd, J. F. J. *Practical Aspects of Ion Trap Mass Spectrometry v.I Fundamental Ion Trap Mass Spectrometry*; CRC Press: New York, **1995**.

Mathieu, E. *J. Math. Pure Appl.* **1868**, *13*, 137.

McLuckey, S. A.; Glish, G. L.; Asano, K. G. *Anal. Chim. Acta* **1989**, *225*, 25-35.

Naito, Y.; Inoue, M. *Int. J. Mass Spectrom. Ion Processes*. **1996**, *157/158*, 85-96.

Niessen, W.M.A.; van der Greef , J. *Liquid Chromatography-Mass Spectrometry: Principles and Applications*. Marcel Dekker: New York, **1992**.

Pedder, R.E. Ph.D. Dissertation, University of Florida, Gainesville, FL, **1992**.

Quarmby, S. T. Ph.D. Dissertation, University of Florida, Gainesville, FL, **1997**.

Schwartz, J. C.; Bier, M. E.; Taylor, D. M.; Zhou, J.; Syka, J. E. P.; James, M.; Stafford, G. C. *Proceedings of the 43rd ASMS Conference on Mass Spectrometry and Allied Topics* **1995**, 1114.

Schwartz, J.C.; Syka, J.E.P.; Jardine, I. *J. Am. Soc. Mass Spectrom*. **1991**, *2*, 198.

Senko, M. *IsoPro* v 3.0. MS/MS Software: **1997**.

Silverstein, R.M.; Bassler, G.C.; Morrill, T.C. *Spectrometric Identification of Organic Compounds*, 4th ed.; John Wiley & Sons: New York, **1981**.

Smith, R. D.; Loo, J. A.; Ogorzalek Loo, R. R.; Busman, M.; Udseth, H. *Mass Spec. Rev.* **1991**, *10*, 359-451.

Stafford, G. C.; Kelley, P. E.; Syka, J. E. P.; Reynolds, W. E.; Todd, J. F. J. *Int. J. Mass Spectrom. Ion Processes* **1984**, *60*, 85-98.

Syka, J. E. P. In *Practical Aspects of Ion Trap Mass Spectrometry v.I Fundamentals of Ion Trap Mass Spectrometry*; March, R. E., Todd, J. F. J., Eds.; CRC Press: New York, **1995**, 169-205.

Thompson, M.Q. Chapter 2: Pressure/Flow Relationships in Capillary Gas Chromatography, In Stafford, S.S. (Ed.) *Electronic Pressure Control in Gas Chromatography*, 2nd ed.; Hewlett-Packard Co.: Wilmington, **1994**.

Tucker, D. B.; Hameister, C. H.; Bradshaw, S. C.; Hoekman, D. J.; Weber-Grabau, M. *Proceedings of the 36th ASMS Conference on Mass Spectrometry and Allied Topics* **1988**, 628-629.

Watson, J. T. *Introduction to Mass Spectrometry*; Raven Press: New York, **1985**.

Wong, P.S.H.; Cooks, R.G. *Current Separations* **1997**, *16*, 85-92.

Yost, R.A.; Enke, C.G.; McGilvery, D.C.; Smith, D.; Morrison, J.D. *Int. J. Mass Spectrom. Ion Phys.* **1979**, *30*, 127-136.

BIOGRAPHICAL SKETCH

Joseph James Mulholland, Jr. was born to Catherine Elizabeth and Joseph James Mulholland, Sr. on September 10, 1969 in Philadelphia, PA. He was several weeks overdue at the start, and has been showing up late ever since.

During his early years, Joe was known to be quite a story teller, often entertaining neighbors on their porches with his imaginative tales while trying to catch a cool breeze on a hot summer evening. At St. Bartholomew's elementary school, he was fortunate to encounter teachers who took an interest in this precocious lad and encouraged his intellectual pursuits and undying curiosity.

But, it wasn't until he attended high school at Holy Ghost Preparatory that Joe encountered the field that would interest him the most—chemistry.

Chemistry represented an intellectual challenge that no other subject could. Though difficult, chemistry had a sense of symmetry and logic which Joe appreciated.

After graduating *summa cum laude* from Holy Ghost, Joe attended Ursinus College with the hope of becoming a doctor. He enrolled in the pre-med program, but chose the unpopular chemistry major as the path to reach his goal. During an EMT (emergency medical technician) training class, he realized that test tubes and beakers were easier to deal with than cranky sick people, so he changed his focus away from pre-med and narrowed in on organic chemistry. Under the direction of Dr. William Middleton, Joe learned many valuable lab skills that he put to use after graduation when he was hired by Cephalon, Inc.

While at Cephalon, Joe thrived under the tutelage of solid chemists and good people like Dr. James Diebold and Dr. Mohammed Iqbal. He was given the freedom to learn new things and try new ideas. It was here that Joe decided that analytical chemistry would be his calling. (It was that or tee-shirt sales.)

A transfer from the Research division to the Development group led to numerous gains for Joe. In Development, Joe was exposed to and gained expertise on numerous analytical instruments. It was during this time that Joe met a lonely old co-worker by the name of George "Granddad" Grandolfi. It was a fortuitous meeting for both since it was the start of a now infamous rivalry on (and off) the basketball court. "The Mighty Mule," as Joe was called, vowed never to let "Granddad" get the better of him.

After five wonderful years at Cephalon, Joe returned to his dream of being a doctor, just not one of the medical variety. He applied to the Universiy of Florida (late, of course) and was miraculously accepted at the ninth hour. While there, he worked for Dr. Richard Yost pursuing various aspects of ion trap mass spectrometry.

I certify that I have read this study and that in my opinion it conforms to acceptable standards of scholarly presentation and is fully adequate, in scope and quality, as a dissertation for the degree of Doctor of Philosophy.

Richard A Yost

Richard A. Yost, Chairman
Professor of Chemistry

I certify that I have read this study and that in my opinion it conforms to acceptable standards of scholarly presentation and is fully adequate, in scope and quality, as a dissertation for the degree of Doctor of Philosophy.

John R. Eyler

John R. Eyler
Professor of Chemistry

I certify that I have read this study and that in my opinion it conforms to acceptable standards of scholarly presentation and is fully adequate, in scope and quality, as a dissertation for the degree of Doctor of Philosophy.

Vaneica Young

Vaneica Young
Associate Professor of Chemistry

I certify that I have read this study and that in my opinion it conforms to acceptable standards of scholarly presentation and is fully adequate, in scope and quality, as a dissertation for the degree of Doctor of Philosophy.

Ian Tebbett
Professor of Physiological Sciences

I certify that I have read this study and that in my opinion it conforms to acceptable standards of scholarly presentation and is fully adequate, in scope and quality, as a dissertation for the degree of Doctor of Philosophy.

D H Powell

David Powell
Scientist of Chemistry

This dissertation was submitted to the Graduate Faculty of the Department of Chemistry in the College of Liberal Arts and Sciences and to the Graduate School and was accepted as partial fulfillment of the requirements for the degree of Doctor of Philosophy.

August, 2000

Dean, Graduate School